AN INVESTIGATION OF VELOPHARYNGEAL CLOSURE WITH LINEAR REGRESSION

by

Anish Sana

December, 2015

Director of Thesis: Dr. Nasseh Tabrizi

Major Department: Computer Science

Cleft lip and palate is a common birth defect in the United States. Children diagnosed with this abnormality face difficulties during feeding, hearing and speech. Surgical methods exist to repair the cleft lip and palate but often require subsequent surgeries as children are unable to gain full speech capabilities as they tend to develop hypernasal speech due to velopharyngeal inadequacy. Investigating velopharyngeal closure can help speech pathologists, surgeons and related professionals understand the effect of velopharyngeal anatomy on velopharyngeal function.

In order to accomplish this, several studies have used two dimensional and three dimensional modeling to visualize the velum. Very few attempts have been made to track the velum and plot its movement against time. Image segmentation has been used widely for various purposes. However, its proficiency in tracking the velum is questionable at the moment. Two image segmentation methods, EdgeTrak and the Hidden Markov Model, are reviewed in this report. EdgeTrak, a software developed at the Video/Image Modeling and Synthesis Laboratory, has been proven to track the surface of a human tongue during speech production. An attempt was made to similarly track the velum during speech production using EdgeTrak but the results were disappointing. Also, synchronized audio mapping using the Hidden Markov Model was only

partially successful. This report describes the challenges image segmentation faces with regards to tracking the velum.

To tackle the ineffectiveness of image segmentation for studying the velopharyngeal system, this study introduces a novel method to investigate the effects of muscles in the velopharyngeal system on closure force using a machine learning algorithm called multiple linear regression. Velopharyngeal muscle data from ten adults and ten children was acquired to train the algorithm. A mechanical representation of the velopharyngeal system was used to calculate the closure force and angle values for the training set which was validated using linearity where closure force increases linearly with increase in muscle activation levels. The algorithm was programmed in MATLAB which used the training set data to predict closure force values and their direction for any set of anatomical parameters. It was observed that the cross sectional area of the velum had a major influence on closure force challenging previous claims that the levator veli palatini was responsible for this. It was also found that the levator veli palatini muscle had a greater influence on closure force direction than other anatomical parameters suggesting that it acts a supporting structure.

AN INVESTIGATION OF VELOPHARYNGEAL CLOSURE WITH LINEAR REGRESSION

A Thesis

Presented To the Faculty of the Department of Computer Science

East Carolina University

&

The Faculty of the Department of Communication Sciences & Disorders

East Carolina University

In Partial Fulfillment of the Requirements for the Degree

Master of Science in Software Engineering

by

Anish Sana

December, 2015

AN INVESTIGATION OF VELOPHARYNGEAL CLOSURE WITH LINEAR REGRESSION

by

Anish Sana

APPROVED BY:

DIRECTOR OF THESIS: _____
Nasseh Tabrizi, PhD

COMMITTEE MEMBER: _____
Jamie L. Perry, PhD

COMMITTEE MEMBER: _____
Sergiy Vilkomir, PhD

CHAIR OF THE DEPARTMENT OF COMPUTER SCIENCE: _____
Venkat N. Gudivada, PhD

DEAN OF THE GRADUATE SCHOOL: _____
Paul J. Gemperline, PhD

DEDICATION

I dedicate this thesis to my friends who helped me maintain my sanity and guided me through every obstacle. I would also like to thank my family who believed in me and supported me in every way possible.

ACKNOWLEDGMENTS

I would like to express my gratitude to my advisor, Dr. Nasseh Tabrizi, for the continuous support of my thesis and related research, for his patience, motivation, and immense knowledge. His guidance helped me in all the time of research and writing of this thesis. I could not have imagined having a better advisor and mentor for my thesis study.

I would also like to thank Dr. Jamie L. Perry, who provided me an opportunity to work on her on-going research, and who gave access to the laboratory and research data. Without her support and guidance, it would not be possible to conduct this research.

TABLE OF CONTENTS

LIST OF TABLES

LIST OF FIGURES

LIST OF EQUATIONS

LIST OF SYMBOLS

N – Newton

lb. – Pound

E – Young’s modulus

λ – Muscle activation level

β – Regression coefficient

ε – Error term

π – Pi

kPa – Kilo Pascal

° - degree

mm – Millimeter

Σ – Summation

g - Grams

LIST OF ABBREVIATIONS

VP distance – Velopharyngeal port distance

Velum-LVP Angle – Velum - Levator veli palatini angle

LVP CSA – Levator veli palatini cross sectional area

VP width – Velopharyngeal port width

F – Force

F_v – Velum force

F_{lvp} – Levator veli palatini force

F_{lvpx} – Levator veli palatini force along the x-axis

F_{lvpy} – Levator veli palatini force along the y-axis

F_{lvpz} – Levator veli palatini force along the z-axis

F_c – Closure force

F° - Closure force angle

F_{cy} – Closure force along the y-axis

F_{cz} – Closure force along the z-axis

CSA – Cross sectional area

CSA_v – Velum cross sectional area

CSA_{lvp} – Levator veli palatini cross sectional area

y – Dependent variable

x – Independent variable

O-O – Origin to origin distance

Sub – Subject

Avg. – Average

STD – Standard deviation

PREFACE

At a time when majority of advancements in technology are focused on creating gadgets that make life easier on a daily basis, I am so grateful to have had the opportunity to use Computer Science on a Health Sciences problem. This interdisciplinary research is the product of the Department of Computer Science's collaboration with the Department of Communication Sciences and Disorders at East Carolina University. I hope this research work can help health professionals and researchers make progress in the treatment of children with cleft lip and palate.

CHAPTER 1 – INTRODUCTION

Cleft Palate is one of the most commonly occurring birth defects. It occurs during embryonic development where a fissure is formed in the midline of the palate due to failure of the two sides to fuse [1]. Normal velopharyngeal anatomy consists of several muscles which includes the levator veli palatini and the velum. These muscles are of particular interest as they aid in velopharyngeal closure, which is essential for speech production and swallowing. Velopharyngeal closure is achieved by retraction and elevation of the velum due to contraction of the levator veli palatini muscle. In children with a cleft palate, the levator veli palatini is attached onto the lateral and posterior aspect of the hard palate which leads to several complications such as feeding, hearing and speech, among others [2]. Even with corrective surgery to restore anatomy, patients are sometimes unable to gain full speech due to velopharyngeal inadequacy which is characterized by hypernasality and sometimes require secondary surgery [3].

Studies examining the variability in velopharyngeal muscle measures in normal individuals [4, 5] did not adequately investigate the effects of this variability on normal and abnormal function. The problem with using magnetic resonance images for such studies is that the samples are small and homogenous which makes it difficult to establish a connection between variable anatomies and their effect on velopharyngeal function. To overcome this problem, quantitative anatomical information obtained from magnetic resonance images, velum and skeletal muscle properties were integrated into a computational model to investigate the effects of variation in velopharyngeal anatomy in normal individuals on velopharyngeal function [6].

Although computational modeling was successful in being able to scale studies by simulating data despite the unavailability of a patient's anatomical data, the technology is not without its drawbacks. The primary purpose of most studies related to the velum are to help speech

pathologists, surgeons, related professionals and researchers make informed decisions. Computational modeling software are expensive, and their usage requires a certain level of expertise and understanding of mechanics.

For these reasons, this study used a machine learning algorithm, multiple linear regression, which took anatomical velopharyngeal parameters as an input to predict the closure force generated and its direction. Normal speech production is attained by velopharyngeal closure which may be influenced by specific dimensional features of velopharyngeal anatomy [2, 4]. Closure force is defined as the force generated in the velopharyngeal system against the posterior pharyngeal wall by retraction and elevation of the velum due to contraction of the levator veli palatini muscle. Multiple linear regression was used in this study, a subset of regression analysis, where one dependent variable is predicted by multiple independent variables [7]. The advantage of this method is that it is entirely data driven. A user wanting to predict the closure force and direction has to only enter the velopharyngeal muscle dimensions into the program.

The information presented in this thesis report is also presented in the papers, “A Review of Image Segmentation Techniques for Tracking the Velum” (accepted by the International Conference on Computational Science and Computational Intelligence) [8] and “Investigating Velopharyngeal Closure Force with Linear Regression” (submitted to the IEEE International Conference on Biomedical and Health Informatics) [9].

The thesis report will unfold as follows –

- Chapter 2 will provide the background where the anatomy of the velopharyngeal system, its effect on speech production, and relevant studies are explored in detail.

- Chapter 3 will explain the ineffectiveness of Image Segmentation for studying the velopharyngeal system.
- Chapter 4 will introduce Linear Regression, the algorithm being used in the study, the methodology and the computer program built to accommodate the methodology.
- Chapter 5 will validate the methodology through the results produced.
- Chapter 6 will discuss the effect of velopharyngeal anatomy on velopharyngeal function through the results found and compare the findings with previous studies.
- Chapter 7 will include the conclusion and provide recommendations for future work

CHAPTER 2 – BACKGROUND

As explained in [2], the orientation of the velopharyngeal mechanism consists of the musculus uvulae that extends from the posterior surface of the hard palate to the posterior pharyngeal wall. It also includes the velum, lateral pharyngeal wall and posterior pharyngeal wall. The velopharyngeal port is the orifice behind the velum which is the distance the velum and the pharyngeal walls must travel to produce speech. The posterior one-third of the velum varies across individuals which affects velopharyngeal closure. The function of the velopharyngeal system is to separate the oral and nasal cavities by sealing the velum and pharyngeal walls during speech production. The oral surface is against the back of the tongue during breathing and elevates to contact the pharyngeal wall during speech. Figure 2.1 shows the velopharyngeal mechanism at rest and during speech production.

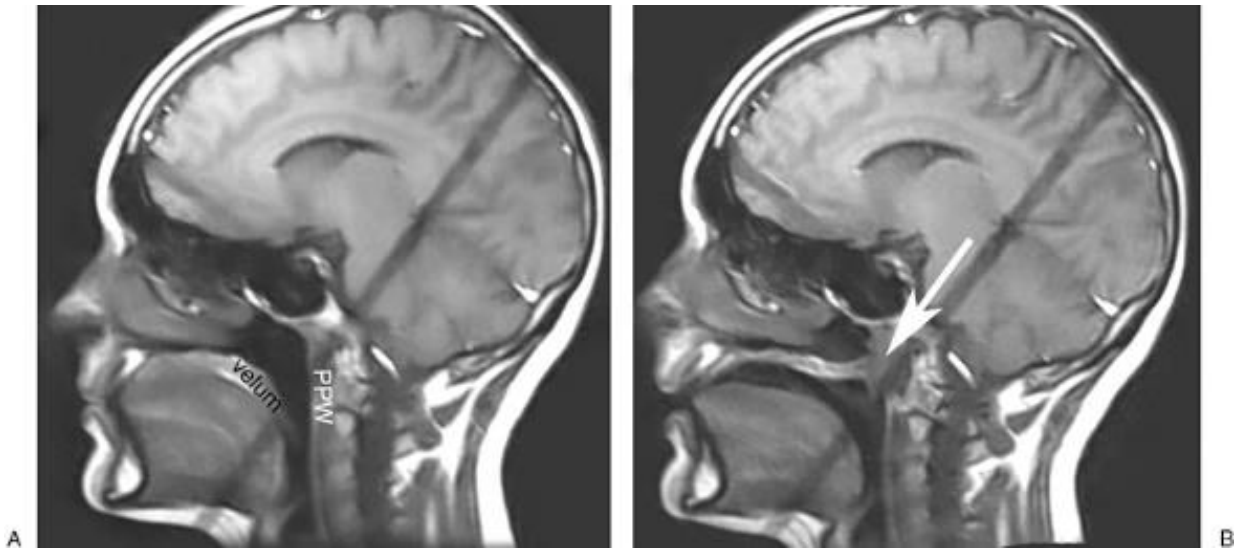

Figure 2.1 – Velopharyngeal mechanism at rest (A) and during speech (B) [2]

A structure called the Passavant's ridge exists in some individuals which bulges forward during speech. The levator veli palatini muscle causes closure by elevating the velum. It originates from the skull to the middle of the velum. The musculus uvulae is situated between the levator veli

palatini and originates from the palatal aponeurosis which supports the velum and regulates jaw movement. It fills the gap between the velum and the pharyngeal walls to ensure better closure. Figure 2.2 shows the internal model of the velopharyngeal mechanism from a lateral and dorsal view.

Figure 2.2 – Internal model of the velopharyngeal mechanism [2]

The tensor veli palatini originates from the scaphoid fossa and lies between the pterygoid fossa. It aids in the opening of the Eustachian tube. The superior pharyngeal constrictor muscle aids in closure of the velopharyngeal system and also might aid in velar refraction. The palatopharyngeus muscle consists of vertical and transverse fibers that aid in lateral pharyngeal wall displacement and positioning of the velum. The palatoglossus runs along the lateral margins of the velum to the lateral part of the tongue. It aids in lowering the velum, elevating the posterior part of the tongue, and constricting the faucial isthmus, thereby allowing a person to swallow bolus. The salpingopharyngeus muscle is located along the lateral pharyngeal walls where it can produce a superior pull but is usually insignificant. Motor innervations of the velum are caused by the trigeminal nerve and the pharyngeal plexus of nerves. Sensory innervations are performed by cranial nerves. Muscle spindles act as sensors which detect change in a muscle's length. Children

with a cleft palate have an absent midline tissue where most of the muscles in the velopharyngeal system are inserted. Due to the absence of the midline tissue, the levator veli palatini is forced to attach itself to the lateral and posterior parts of the hard palate. Also, the musculus uvulae is reduced in size, present in a different location or completely absent. Due to these issues, children face problems during feeding, hearing and speech. Figure 2.3 shows an unrepaired unilateral cleft lip and palate where the levator veli palatini muscle is attached to the hard palate.

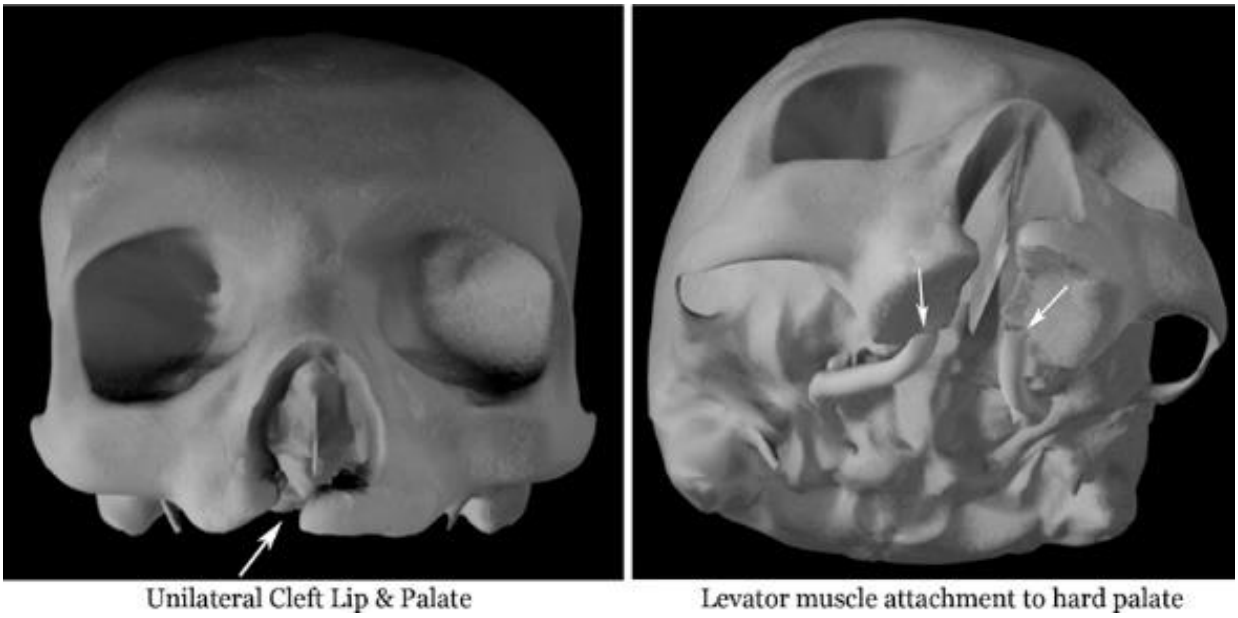

Figure 2.3 – Cleft palate [2]

Several studies have investigated the velopharyngeal system with various techniques. Finite Element Modeling predicted realistic geometries of the velum during velopharyngeal opening and closing using a two dimensional computational model [10]. The study decided to use a two dimensional model instead of a three dimensional one to avoid unnecessary complications. Velar dimensions were measured of which the anterior border was fixed and the rest remained unrestrained. The model was split into elements such that they were as square as possible which helped in numerical stability. Results from a histological study were mapped into the model and

the tissue strain and stretch were predicted when stress was applied. The young's modulus that was used for tendinous tissue was lower than what was used in their reference literature in order to produce sufficient bending near the anterior boundary. The young's modulus for some tissues were unavailable and hence were hypothesized. Histological studies provided the location for velar muscles and the forces from external muscles exerted on the velum. Hooke's law was avoided due to large strains in the system and the Neo-Hookean equation was modified so that the system was nearly incompressible instead of being strictly incompressible because velar tissues contain water. ABAQUS [11] was used to simulate the finite element model where the initial velum shape, equations and external forces were provided as inputs and the deformed velopharyngeal configuration was deemed to be the output. The study showed that constriction of the palatoglossus muscle caused velopharyngeal opening and the assumption of incompressible tissues warranted the use of second order quadratic elements which caused the velar shape to look rugged. Levator veli palatini helped in velopharyngeal closure which generated a force of 0.29 N distributed across all elements. The palatopharyngeus muscle also aided in velopharyngeal closure producing a force of 0.029 N, which is one-tenth of the force generated by the levator veli palatini muscle in all instances, even though one does not necessarily cause the other. The distance between the velum and the posterior pharyngeal wall decreases linearly with an increase in the velar force exponentially. The study also supported a theory that the soft palate continues moving upwards along the posterior pharyngeal wall after initial contact. It was also found that a large force from the palatoglossus muscle causes the velum to lower further.

An approach where speech dependent articulatory adjustment for hypernasality based on data from electromagnetic articulography was developed to reduce hypernasality [12]. Nasalization is the result of air passed out through the naval and oral cavities when the velum is

lowered. Nasalization due to velopharyngeal inadequacy is common in patients with a cleft palate. Corrective surgery can be used to overcome the cleft palate but speech therapy is required to correct the resulting misarticulation. Speech therapy is often based on the perception of the therapist but in reality, the treatment needs to be customized which was the aim of this study, where the patient can learn techniques to reduce the perception of hypernasality. A pilot study was conducted where the participants of the study consisted of speakers and listeners of American English with no speech and hearing disabilities. The subjects were asked to sustain a speech sample which consisted words of the consonant-vowel-consonant form. The speech samples were used to compute acoustic targets, minimize discrepancy, create a voice source and perform a synthesis. The speech samples were segmented into vowels, namely – oral, nasal, and nasal with articulatory adjustment, to be used as acoustic targets and normalized to eliminate frequency differences between speakers. Both speakers and listeners were trained to familiarize themselves with the speech quality and their perception of nasality, respectively. It was seen that articulatory adjustment caused the vocal tract to expand in various areas. The plotted nasality scores were lower than nasal vowels without articulatory adjustment and higher than oral vowels. Excessive velopharyngeal opening causes acoustic deviation which is compensated by articulatory adjustment along with reduction in perceived nasality. The model only worked for the speaker of the speech samples. It needed to be normalized to make it applicable to other speakers. The model was modified by conducting two experiments. The first experiment acquired articulatory data and audio signals. The second experiment estimated the velopharyngeal opening using the hydrokinetic method based on electropathography recordings and aerodynamic speech signals. Nasal airflow, intraoral pressure and nasal pressure were measured. The articulatory data was used to adapt the vocal tract model for two speakers by aligning and normalizing the coordinate system

and adjusting the articulatory parameters. The audio signals and simulated speech were compared and any mismatches were adjusted manually which helped in adapting the model for speaker variability. Movement ranges of articulators were used to create a speaker dependent articulatory space which was used is customizing the model. In experiment 3, participants listened to the stimuli after listening to their respective moduli in order to rate nasality using direct magnitude estimation. It was found that the first three orthogonal nodes accounted for over 95% variance in the nasal oral area functional difference for all vowels and speakers. Vowel types had a significant effect on nasality. The mean nasality score of adjusted nasal vowels was found to be lower than that of unadjusted nasal vowels and higher than that of oral vowels. The results from the study enabled the researcher to make comparisons between oropharyngeal articulations of oral and nasal vowels. The correlation between the logarithm of equalized nasality scores and the amplitude of coefficients showed a significant correlation between nasality and adjusted nasality. Nasalization resulted in oral and nasal articulatory differences. Lowering of the velum influenced nasalized vowels. The phonetic event of nasalization included velar lowering and oropharyngeal articulatory adjustments which defined the shape of the vocal tract. Patterns of articulatory adjustments and movement of articulators in nasalized vowels were in contrast with oral vowels and resulted in variations in oropharyngeal articulation. The study suggests that adjustment in oropharyngeal articulation can compensate for the effects of velar lowering. The study successfully used a speaker adaptive model to perform articulatory adjustment to compensate for the acoustic outcome due to excessive velopharyngeal opening. Also, the model was customized with speaker dependent features to account for speaker variability. It also caused a reduction in nasality rating which suggests that the perception of nasality was reduced. The study will be helpful to train patients

with velopharyngeal inadequacy to properly articulate their speech to reduce the perception of nasality.

The Hidden Markov Model was combined with synchronized audio mapping using Mel Frequency Cepstral Coefficients to track the velum and pharynx during speech production from dynamic magnetic resonance image data [13]. Images were captured at a fast rate while producing the word “ansa” which ensured that images of the velum were captured at different positions. A metronome beat was used to control the rate of speech. Care was taken to isolate areas with high fat concentration and imperfections resulting from the magnetic field in the oropharyngeal region. These images were reconstructed ensuring that there was no redundancy and blurring was minimized, after which they were aligned with their respective audio. The audio feature extraction was performed by importing magnetic resonance images and isolating the audio and images. Noise removal, Mel Frequency Cepstral Coefficients and feature discretization was performed on the audio. The images were also tagged, normalized and reduced in order to train the hidden markov model for prediction. Visual features were extracted using four markers and one stationary pivot point. The anterior and posterior pharyngeal wall movement was calculated along the horizontal axis. Three hundred sequential images were tagged which showed movement in the X-Y coordinate system. The hidden markov model was used to predict velar and pharyngeal wall boundaries. The audio features were observations (inputs) to the model whereas video features were the hidden states (outputs). MATLAB [14] was used to estimate the hidden markov model parameters for each marker. Two hundred audio features’ data sets were used to train the model and a hundred samples were used for testing. The most likely sequence of hidden states was then predicted. The location and shape of the velum and pharyngeal wall was predicted using Accumulative Minimum Distance and Evaluation by Inspection. The former is a mathematical

approach which calculates the difference between actual and predicted distance. This proved to be inaccurate due to researcher induced errors as the result was equal to or greater than the accumulative minimum distance. The study found that fewer hidden states resulted in less residual in the prediction result. Also, little movement in the pharyngeal wall results in a smaller error rate. A correlation was found between the audio signal amplitude and the error rate, where a higher amplitude resulted in a higher residual in the prediction result. Higher velocity in the velum caused an increase in error rate during speech production as the velum moved too fast while contacting the pharyngeal wall for only a very short duration. Evaluation by inspection was a comparison done by the researcher between manual markers and superimposed predicted markers, where the acceptance rate was found to be 83%.

Magnetic resonance imaging has been used extensively in combination with other technologies such as Electropalatography to study inter and intra-speaker variabilities in articulatory dynamics [15], where it was concluded that magnetic resonance images were useful for three dimensional vocal tract modeling and measurements whereas electropalatography accounted for speaker variability.

Magnetic resonance imaging was also combined with Computed Tomography imaging to develop a three dimensional linear articulatory model of the velum [16]. An organ based model was developed where each organ was modeled separately after which the oral and nasal tracts were modeled. Non rigid organs were modeled using the weighted sum of nonlinear components which were extracted using principal component analysis and linear regression. The weighted sum included articulatory control parameters which defined the shape of organs. The study developed a database of shapes and analyses of their corresponding three dimensional coordinates. The corpus consisted of artificially sustained articulators with supplementary rest and prephonatory

articulators. A computed tomography scan of the head was performed where images were taken at rest to locate bony structures. Similarly, magnetic resonance images were obtained while the subject sustained articulations which determined soft tissues. Due to the low resolution of images, manual extraction of contours was performed. The computed tomography and magnetic resonance images were resliced. Bony structures were determined through manual edition of each organ plane by plane and expansion of two dimensional contours into a three dimensional coordinate system. The three dimensional reference coordinate system was attached to the subject's skull. Computed tomography images were manually aligned which provided six degrees of freedom, called three dimensional rototranslation which was performed using MATLAB [14] to account for the subject's head movement while the images were being taken. Similar to the technique used to determine bony structures, magnetic resonance images were used to determine soft structures. A three dimensional surface mesh was fitted to the elastic deformation of three dimensional shapes during articulation which helped in the modeling. The elastic deformation was calculated to create a set of soft and hard organ surfaces which were used for articulatory modeling. The study established an articulatory model of the velum by applying direct principal component analysis to observed velum shapes which extracted articulatory control parameters that determined the involvement of the levator veli palatini muscle and closure mechanism of the velum.

Recent studies have focused on combining magnetic resonance images with three dimensional modeling such as studying the velopharyngeal anatomy of infants with and without a cleft palate [3], where the project aimed to better understand the velopharyngeal structure by combining magnetic resonance imaging and computer imaging technology. A three dimensional computer model and animation of the velopharyngeal system was created which could be used by a researcher to view the system in all coordinate planes, apply external forces and chart resultant

movements. The levator muscle dimensions obtained from quantitative magnetic resonance imaging data were used to model the system using a software called Maya [17]. The project successfully created a two minute animation of velar movement.

Several limitations exist in modeling the velopharyngeal system such as modeling soft tissue structures based on data gathered from computed tomography scans. These challenges were addressed by the use of magnetic resonance imaging and quantitative data [18]. An animated model was created to show velar movement at rest and during speech. Using the software Maya [17], polygonal structures were used to model the muscles. The quantitative data used consisted of static measures and magnetic resonance images that were taken in different planes. Since the measurement of the levator muscle was not obtained from dynamic data, linear interpolation was used. It was ensured that the model matched the data sets and a skull was fit to outline the model and add realism.

A similar modeling study [19] was conducted to study the velopharyngeal anatomy of infants with and without a cleft palate. Magnetic resonance images were taken of all subjects with a fully functioning velum and one subject who had hearing loss. Subjects with a cleft palate were scheduled to receive corrective surgery. Two dimensional scans were performed in different planes at high resolutions and similar consistency. The magnetic resonance images were fed into a three dimensional visualization software which ensured that no errors were imported when transferring data between programs. The software allowed for segmentation of muscles of interest which were imported into Maya [17] preserving their original quality. Less important structures to the velopharyngeal system such as the skull were modeled based on magnetic resonance imaging data. Computer models were created for all subjects which included after surgery models for subjects with a cleft palate. Animations of the surgical procedure were also created and joined together to

create an instructional movie before surgery. Several variations were observed by combining magnetic resonance images and computer modeling, such as differences in the levator muscle sling arrangement, levator fibers' attachment, velum length, angle of the levator muscle, location of the uvula and other minor tissue variations.

All of the literature mentioned in the chapter have been an improvement over the other in a chronological order. The latest techniques have used magnetic resonance images as a staple. Therefore, attempts were made to use image segmentation to track the velum, details of which are provided in CHAPTER 3.

CHAPTER 3 – IMAGE SEGMENTATION

Image segmentation can be used to detect objects where the goal is to cluster pixels into salient image regions using methods such as thresholding, clustering, histogram based, edge detection and stereovision based, among others [20].

Edge detection is one such method where image segmentation is performed based on the discontinuity in images that are spliced when an abrupt change in intensity occurs in the edges of an image [21]. Several edge detection techniques are currently in existence but a novel method called EdgeTrak was specifically developed by the Video/Image Modeling and Synthesis Laboratory to track a human tongue [22]. The method was successful in tracking the human tongue due to which, a study was conducted to enquire whether it can be used to track muscles other than the tongue, specifically the velum. This proved to be a failure for which the reasons are detailed in this chapter.

Additionally, another study is reviewed in the chapter where image segmentation was combined with a machine learning technique called the Hidden Markov Model to track the velum [13]. In a hidden markov model, the state at some time encapsulates all information about the process in order to predict the future of that process [23]. Using this technique, the study tried to map movement in magnetic resonance images with its corresponding audio. A success rate of 81% was achieved in predicting velar movement. However, this is insufficient from a clinical standpoint as the purpose of tracking the velum is to obtain information on its movement with regards to speech that can be used to treat velopharyngeal inadequacy.

EdgeTrak was a software developed to automatically track the surface of a human tongue in a sequence of ultrasound images which is a challenge due to noise and unrelated high contrast edges in ultrasound images. Instead of using only the gradient of images such as the image force, EdgeTrak uses edge gradient and intensity information in local regions around snake elements. One of the advantages is that EdgeTrak can be used with open contours and track partial tongue surfaces whereas others can only be applied to closed contours. Also, any unnecessary edges are discarded. The software was successfully able to track the surface of a human tongue in ultrasound images as shown in Figure 3.1 [24].

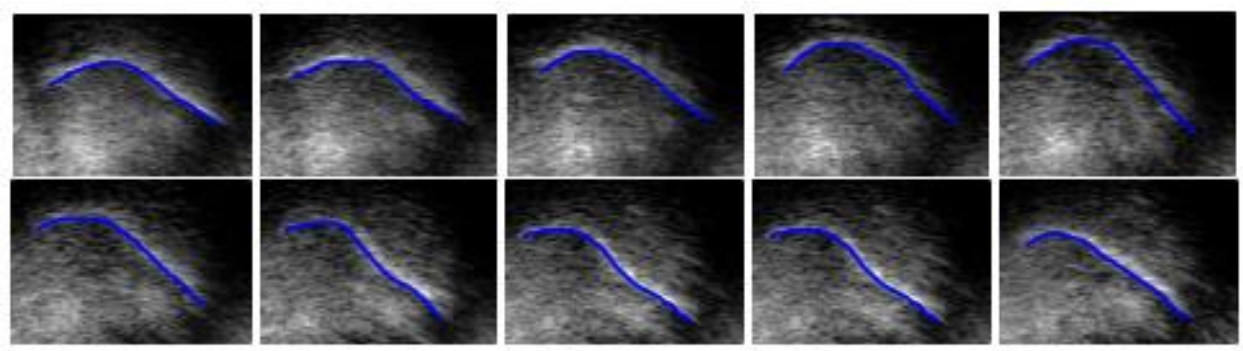

Figure 3.1 – EdgeTrak tracking the surface of a human tongue [24]

Given the success of EdgeTrak in tracking the human tongue surface, it was hypothesized that it could be used to similarly track the velum. An eight second video of a child with normal anatomy uttering the phrase “pick up the pup” was used as shown in Figure 3.2.

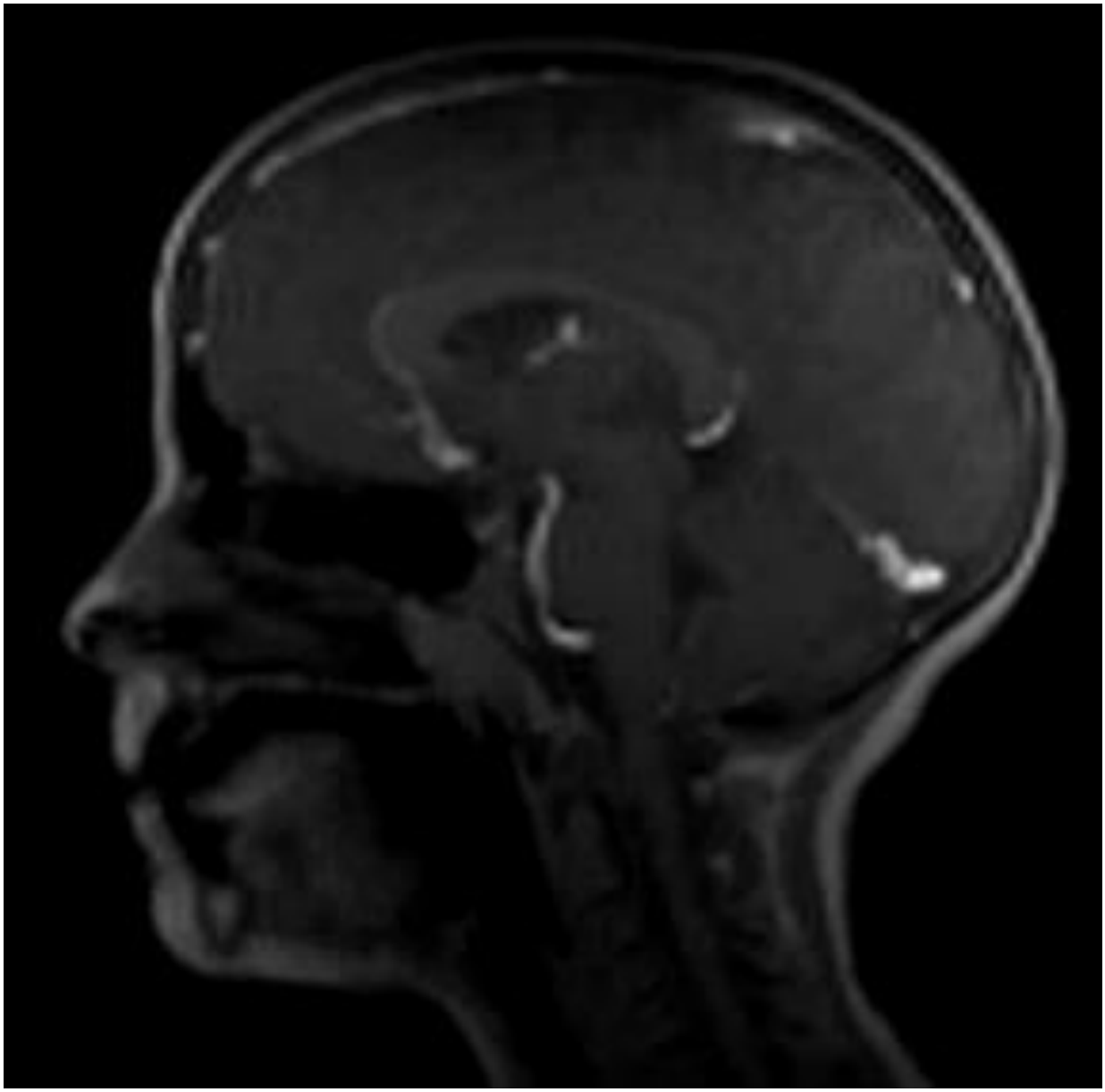

Figure 3.2 – Image from the video of a child saying “pick up the pup”

This video was originally compiled from a sequence of magnetic resonance images. The video was split into two hundred and fifty sequence of images using the software Blender as shown in Figure 3.3 [25]. These images were then cropped to the region of interest using MATLAB [14].

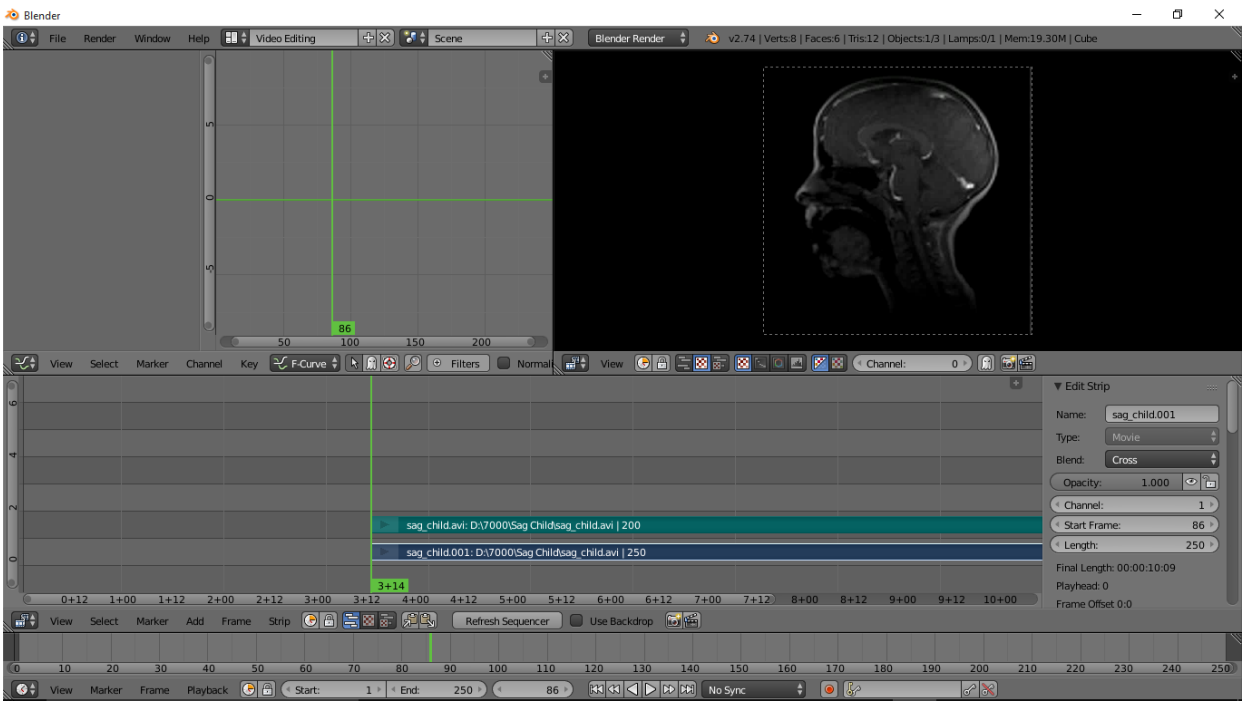

Figure 3.3 – The software Blender generating image sequences from videos

The cropped images were loaded onto EdgeTrak and snake initialization was done on the velum as shown in Figure 3.4. EdgeTrak was then allowed to automatically track the velum through all images in the uploaded image sequence.

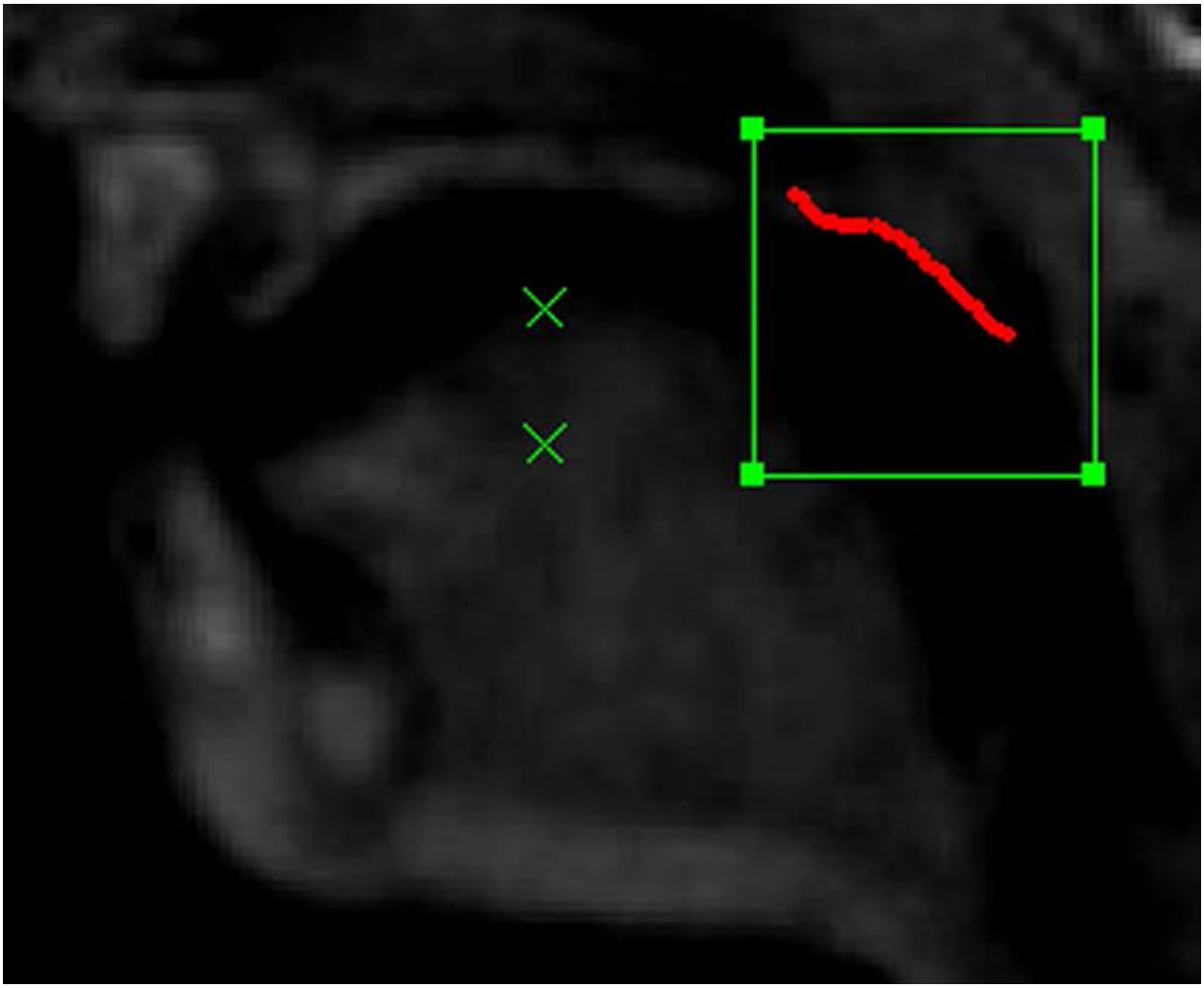

Figure 3.4 – Snake initialization on Edge Trak

Image quality is a major concern while using EdgeTrak. In sequence 1 as shown in Figure 3.5, the velum is clearly visible in all instances due to which the software was able to efficiently track it.

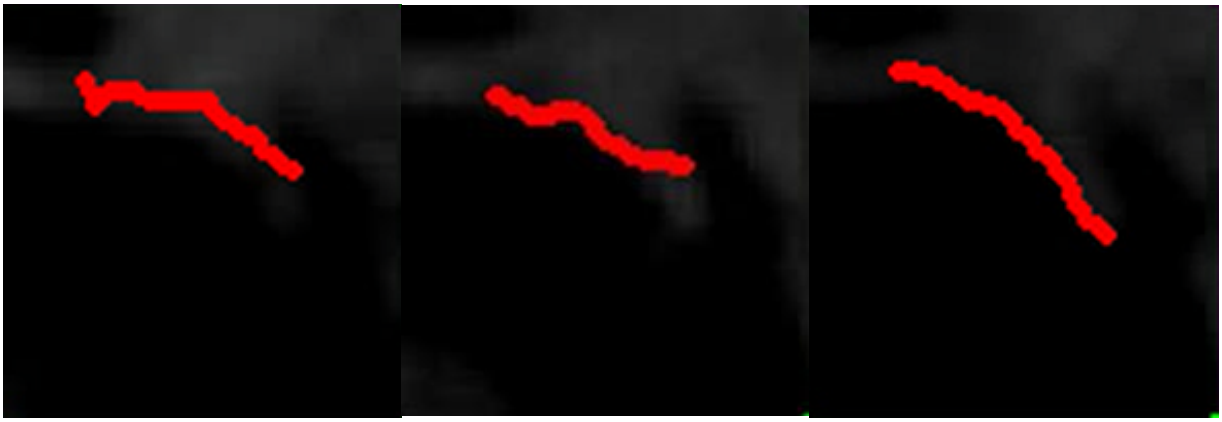

Figure 3.5 – Snake tracks the velum successfully

EdgeTrak relies on image intensity to track its objective. One of the problems with using image segmentation to track the velum has been that the velum and the posterior pharyngeal wall have the same intensity. As it can be seen in sequence 2 shown in Figure 3.6, the snake gets attracted to the posterior pharyngeal wall and gets lost, due to the posterior pharyngeal wall's intensity being similar to that of the velum.

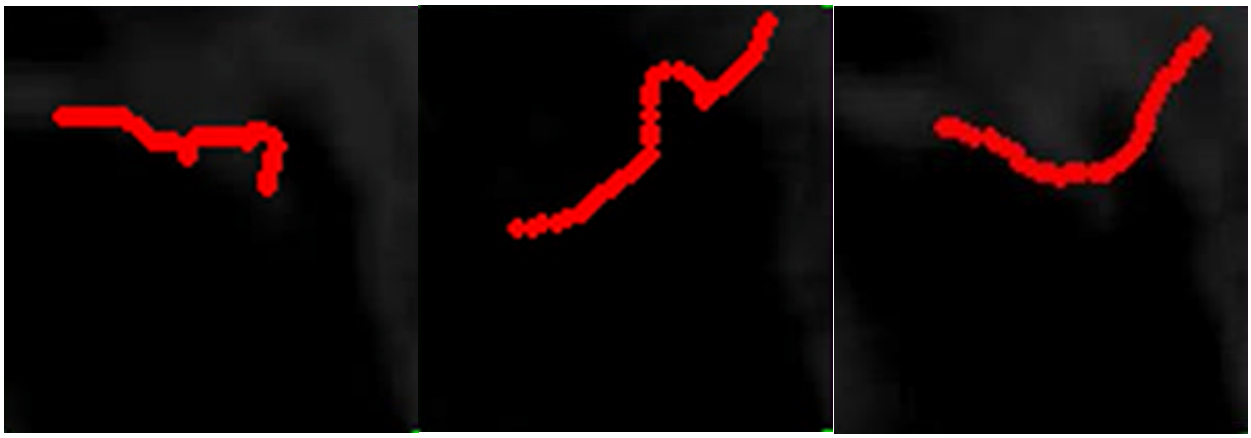

Figure 3.6 – Snake gets attracted to the posterior pharyngeal wall due to similar intensity

As mentioned previously, image quality is important for the software to track the velum. In sequence 3 as shown in Figure 3.7, the velum disappears, due to which the size of the snake shrinks.

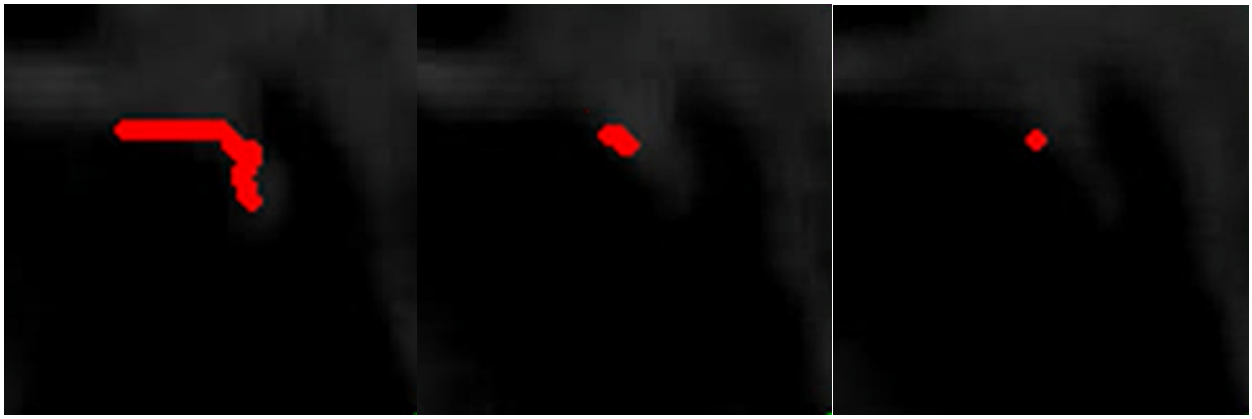

Figure 3.7 – Snake shrinks due to the velum disappearing

Another major concern with EdgeTrak is consistency. Sequence 4 as shown in Figure 3.8 shows the snake tracking the velum for the same sequence of images used in sequence 3, but noticeably getting smaller with each successive image and later regaining its size. This is clearly undesirable as results cannot be duplicated. One reason for this inconsistency is that EdgeTrak requires a human to manually initialize the snake and then tracks its objective based on initialized image intensity. A small error during initialization could cause the snake to show variability in its tracking. However, this is very unlikely to avoid as it is difficult for the human eye to select the same two pixels on an image.

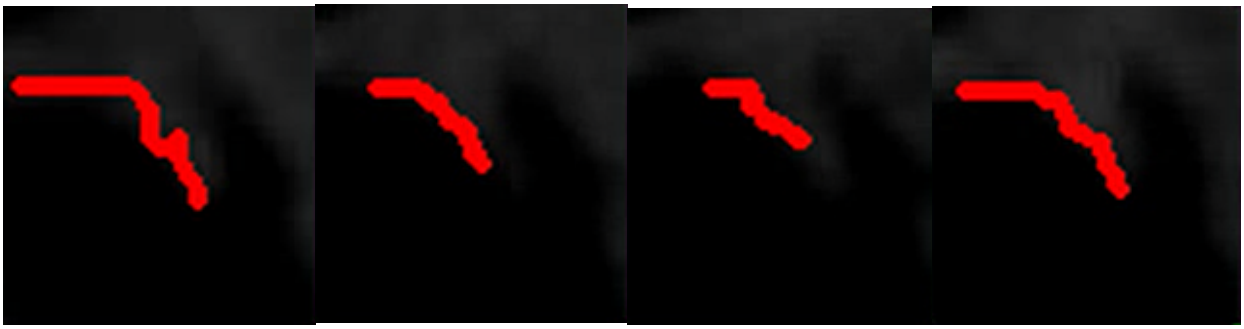

Figure 3.8 – Snake showing inconsistency while tracking the same set of images

Additionally, EdgeTrak can only be used on a limited number of images due to memory constraints. The manual [26] provided during installation states that less than or equal to eighty images should be used but as image size is increased, the number of images that can be used decreases.

The hidden markov model has been widely used to track objects. Researchers at Lund University [27] were successfully able to track multiple objects using the hidden markov model in image sequences on three different setups – footfall counter, parking lot monitor and car tracking in traffic surveillance videos. The parking lot setup was an initial test where the entrance to a narrow parking lot was monitored over seven hours and consisted of seventeen events. All but one of the events were correctly detected, giving it an error rate of 3.6%. In the footfall setup, people entering and leaving a building were counted by tracking each person for a short distance to decide if the person was entering or leaving, with an accuracy rate of 96.4%. In the traffic setup, a seven minute surveillance video was analyzed consisting of fifty eight cars and several large vehicles, of which fifty seven cars were detected. Not just objects, the hidden markov model can also be used to track signals as shown in a study [28] where the researchers were able to track two slowly varying time tones in additive white Gaussian noise. The hidden markov model can also be combined with other tracking methods, such as Augmenting Electro Optical based tracking systems with Infrared modality, known as Coupled Hidden Markov Model [29]. In this study, the researchers conducted experiments on real world sequences and reported improvement in tracking accuracy over other integration schemes where the target object was corrupted by noise.

The study that aimed to track the velum using the hidden markov model [13] consisted of three hundred images tagged by the researcher of which two hundred images and their corresponding audio features were used to train the model. A two and a half second audio file was

used to test the model where the error rate was considered to be the minimum calculated distance between predicted and actual markers. The model was able to track the velum with an accuracy of 81%. Although this accuracy is high, there are several problems with the model –

- Tracking – An accuracy of 81% means that the model can only successfully track the velum four out of five times. From a clinical standpoint, this is not sufficient. The purpose of tracking the velum is to gauge its movement with regards to speech. This information can then be used by either speech pathologists to train patients with velopharyngeal inadequacy or clinicians to solve velopharyngeal inadequacy through surgical means. For this purpose, the aforementioned accuracy is not sufficient to make informed decisions.
- Human Errors – In the model, the researcher tags the images manually. This induces errors as was self-admitted by the researcher. The images were used to train the model and hence any errors would have continued throughout the image sequence which adds to the model's inaccuracy.
- Performance – Machine learning algorithms such as the hidden markov model perform better with increase in data supplied to the model [30]. Given this, the model can never gain 100% accuracy until it obtains all the data required for future predictions, which in this context would mean the entire population of the planet. This is certainly not possible.
- Repeatability – The predictions made in the study with the aforementioned accuracy are patient dependent. It is difficult to run the model on every patient.
- Cyclical repetitions – The predictions made in the study were of patients uttering speech in cyclical repetitions. In order to be truly effective, the model needs to predict velar movement in regular speech.

These observations are supported by a study performed at François Rabelais University [31], where a new way of using the hidden markov model to track objects in video sequences was developed. The goal was to track a football during the entire length of a shot by predicting the approximate object position using a simple motion estimator first, following which the exact object position was computed. The method yielded a success rate of 87%. It only partially succeeded in tracking objects during occlusion (object of interest hidden partially in an image sequence), and faced difficulties when faced with two similar objects, such as the ball and a sock.

Computer based automatic tracking using image segmentation is often complicated due to the amount of time required to conduct the process and the inherent noise, motion artifacts, air interfaces and refractions in magnetic resonance images. Additionally, poor image quality and lack of a distinct boundary between the velum and the posterior pharyngeal wall make the process even more difficult [13].

EdgeTrak showed a lot of promise given the success it had in tracking the surface of a human tongue. However, the results with regards to tracking the velum have been disappointing. Several challenges remain for the software to be applicable to muscles other than the tongue. It needs to be able to work with images of poor quality as it is not always possible to obtain high quality magnetic resonance images or images of other nature. Its over-reliance on image intensity causes the snake to get attracted to areas other than the region of interest. An option to select the region of interest other than a box would allow the user to select the appropriate region and avoid the snake from getting distracted. An automated method of initializing the snake could help eliminate human error and provide consistent tracking.

Machine learning algorithms such as the review of the hidden markov model performed in this chapter are successful in tracking the velum but possess many limitations. Accuracy is always an issue as the hidden markov model requires large amounts of data in order to be able to successfully predict velar movement that is beneficial for clinical purposes. In this particular study, there was an element of human error which could possibly be avoided in future models with the help of an automatic marker. Then again, having an automatic marker would mean that it is able to successfully track the velum, in which case other efforts are redundant.

Image segmentation can be used for tracking but it is currently unreliable and requires improvement. The technical limitations mentioned can be tackled with improvement in technology. However, theoretical challenges remain which require further research for it to be useful for clinical purposes.

Due to the ineffectiveness of image segmentation, a novel approach to use Linear Regression was undertaken, as described in CHAPTER 4.

CHAPTER 4 – LINEAR REGRESSION

Statistical models describe a state or a process [7]. Regression Analysis is a type of statistical model that investigates the statistical relationships between two or more variables. The variables consist of either one or more independent variables which are used to predict the response variable that is dependent on these independent variables. Regression analysis can be split into two types – linear regression and non-linear regression. Linear regression requires linearity in regression parameters whereas in non-linear regression, the relationship between the independent variables and the dependent variables is not linear, which is why the latter is not applicable to this study since it has been observed that closure force increases linearly with increase in muscle activation [6, 32]. In simple linear regression, one independent variable is used to predict one dependent variable. Equation 4.1 is a simple linear regression algorithm where y is the dependent variable, β_0 is the y intercept, β_1 is the slope of the regression line, x is the independent variable, and ε is the random error.

$$y = \beta_0 + \beta_1 x + \varepsilon$$

Equation 4.1 – Simple linear regression algorithm [7]

Simple linear regression can be taken a step further to attain multiple linear regression where instead of a single independent variable being responsible for the outcome of the dependent variable, there are more than one independent variable that are responsible for the outcome of the dependent variable. Since this study uses a range of muscle parameters for predicting the closure force and its direction, a multiple linear regression algorithm was used as shown in Equation 4.2, where y is the dependent variable, β_0, β_1, …, β_p are regression coefficients, x_1, …, x_p are independent variables, and ε is the error term.

$$y = \beta_0 + \beta_1 x_1 + \cdots + \beta_p x_p + \varepsilon$$

Equation 4.2 – Multiple linear regression algorithm [7]

This study was reviewed and approved by the Institutional Review Board at East Carolina University (IRB #11-001103) and the University of Illinois, Urbana Champaign (IRB #11099) – additional information for which can be found in APPENDIX G. For this study, data was collected from a total of twenty subjects of whom ten were adults and ten were children. This data consisted of muscle dimensions and angles in the velopharyngeal system. The following parameters were used in the training set for linear regression computation, also used in a modeling study [6] that was used for comparison and detailed in Figure 4.1 –

- Velopharyngeal port distance (VP distance) – Anterior to posterior distance of the velopharyngeal port through the midline.
- Velum - levator veli palatini angle (Velum-LVP Angle) – Angle between the velum and the levator veli palatini muscle formed between the line of the oblique coronal plane and the line connecting the posterior nasal spine and levator veli palatini center.
- Velar length – Length of the velum measured from the posterior nasal spine to the velar knee.
- Levator veli palatini cross-sectional area (LVP CSA) – Cross sectional area of the levator veli palatini muscle at the middle.
- Velar thickness – Thickness of the velum at the middle of the levator veli palatini muscle.
- Extravelar length – Length of the levator veli palatini muscle outside the body of the velum measured from its point of origin to the point where it enters the velum.
- Velopharyngeal port width (VP width) – Width of the velopharyngeal port.

- Intravelar segment – Length of the levator veli palatini muscle measured between the points of entry into the velum.
- Origin to origin (O-O) – Distance between the points of origin of the levator veli palatini muscle at the base of the skull.

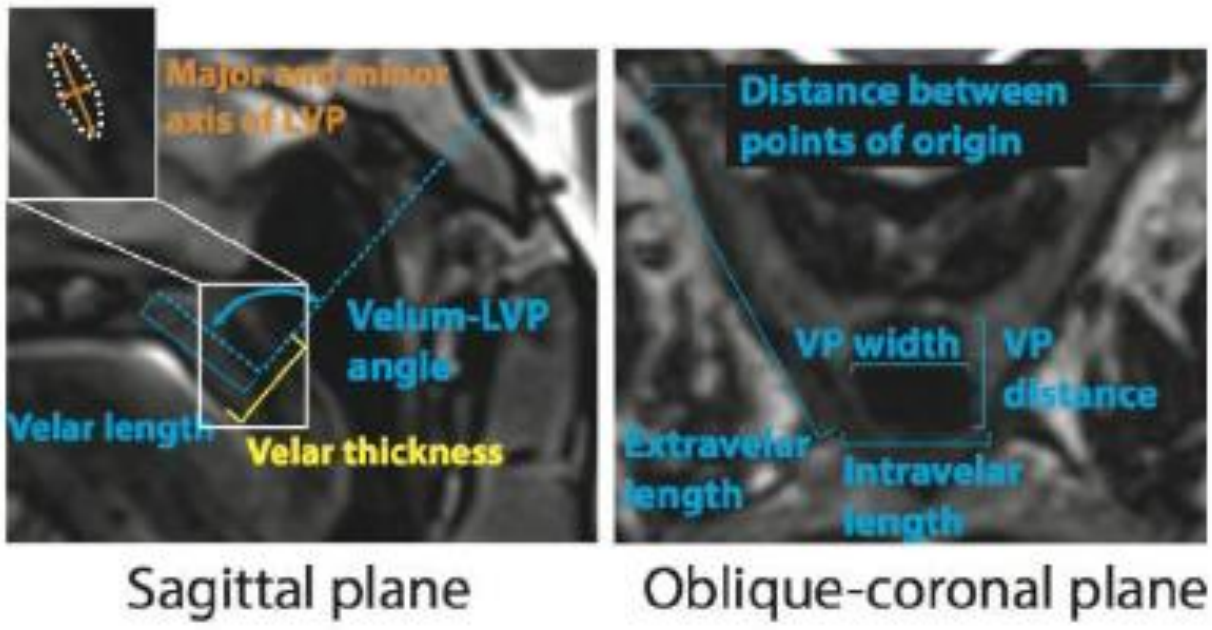

Figure 4.1 – Muscle measurements from magnetic resonance images [6]

There are significant differences between white males and females across several levator muscle measures [4]. To eliminate this effect, all subjects used in the study were white males. Adults aged in the range of 19-22 whereas children were in the range of 8-9 years old. All subjects spoke English as their native language and were devoid of any abnormalities. Table 4.1 displays the demographic information of the subjects used in the study. Detailed demographics of the subjects can be found in APPENDIX A.

Table 4.1 – Subject demographics

Subject code	Age at scan (years)
2	22
10	21
20	20
22	20
31	20
34	22
37	22
38	20
41	22
42	19
Child002	5
Child 005	6
Child 006	5
Child 004	9
543	8
400	8
449	9
448	9
356	9
324	9

Data gathered from these subjects was used to calculate closure force values and the angle at which those forces were acting. Figure 4.2 shows the velopharyngeal system being split into various force components acting on it.

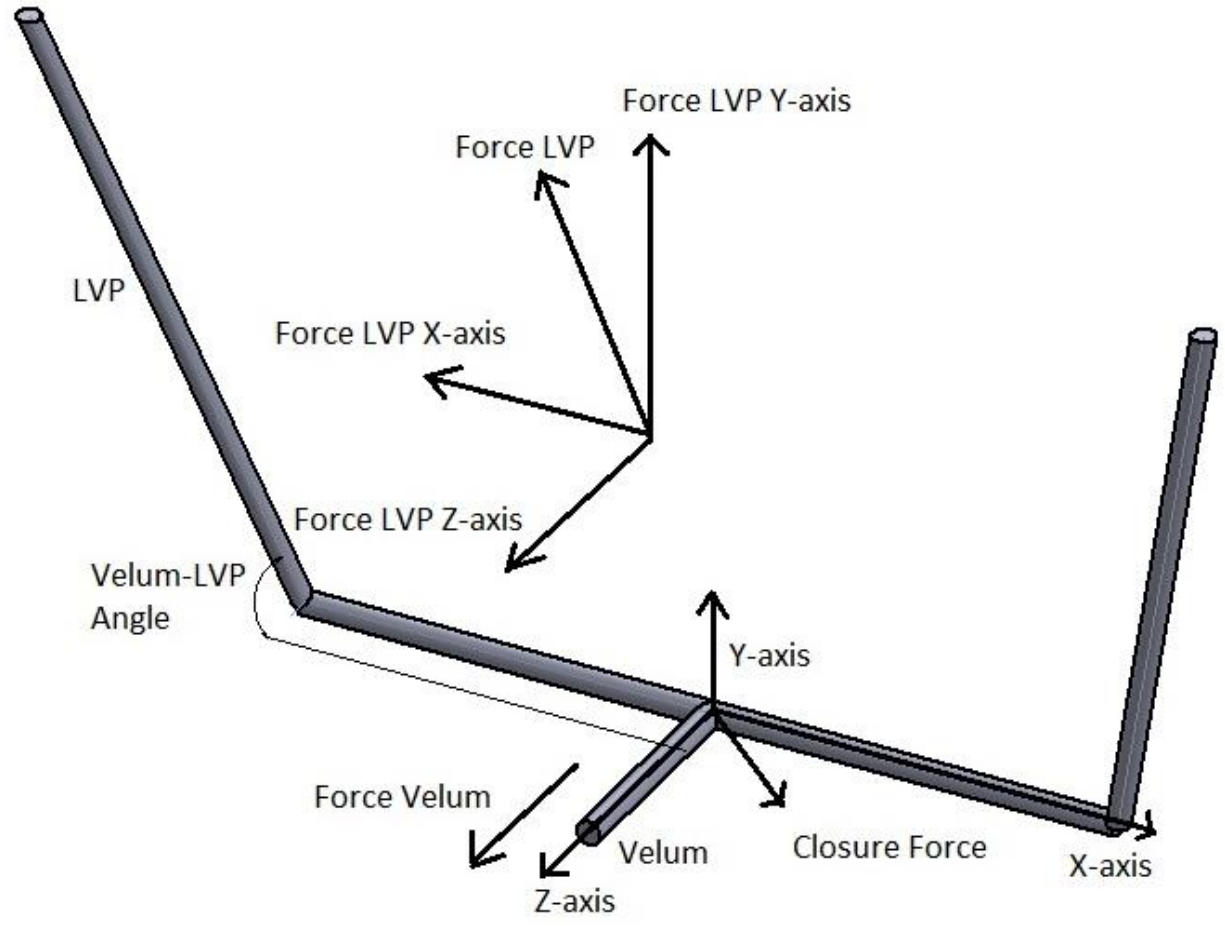

Figure 4.2 – Velopharyngeal system split into force components

The levator veli palatini muscle and velum were modeled as springs with the intravelar segment as the common axis. Velar force (F_v) acts along the z-axis at the middle of the intravelar segment whereas the levator veli palatini force (F_{lvp}) acts along the extravelar segment at either ends of the intravelar segment. Equation 4.3 was used to calculate the force generated by each of the springs where, CSA is the cross-sectional area, E is the Young's modulus, and λ is the activation level.

$$F = CSA * E\ (\lambda - 1)$$

Equation 4.3 – Force calculation [6]

The cross sectional area of the velum (CSA_v) and the levator veli palatini muscle (CSA_{lvp}) were calculated using Equation 4.4 and Equation 4.5, respectively.

$$CSA_v = velar\ thickness * VP\ width$$

Equation 4.4 – Velum cross sectional area

$$CSA_{lvp} = major\ axis * minor\ axis * \frac{\pi}{4}$$

Equation 4.5 – Levator veli palatini cross sectional area

The Young's modulus used in this model was 5 kPa. Previous studies have used Young's modulus values ranging from 0.5 kPa to 100 kPa [10, 33, 34, 35, 36, 37]. The 5 kPa value chosen for this study computes closure force values that agree well with other studies where closure force was found to be ~1N at 100% activation of the velum [6, 32]. The activation level refers to the position of the velum and the levator veli palatini muscle. 0% activation indicates that the muscles are at rest whereas 100% is when they are fully activated, for instance, the velum making contact with the posterior pharyngeal wall. Forces generated by each of the springs was split into their component forces acting along the x, y and z axes. The levator veli palatini forces generated along the x-axis are equal and opposite causing them to negate each other. The component forces on the y and z axes were used to calculate the closure force along the y-axis (F_{cy}) and z-axis (F_{cz}) as shown in Equation 4.6 and Equation 4.7 respectively, where F_{lvpy} and F_{lvpz} were the levator force components in y and z axes , respectively.

$$F_{cy} = -(2 * F_{lvpy})$$

Equation 4.6 – Closure force along y-axis

$$F_{cz} = -[(2 * F_{lvpz}) + F_v]$$

Equation 4.7 – Closure force along z-axis

The resultant closure force (F_c) acted downwards against the posterior pharyngeal wall whose magnitude and angle of direction (F°) were calculated as shown in Equation 4.8 and Equation 4.9, respectively.

$$F_c = \sqrt{F_{cy}^2 + F_{cz}^2}$$

Equation 4.8 – Resultant closure force

$$F^{\circ} = \sqrt{tan^{-1}(\frac{F_{cy}}{F_{cz}})}$$

Equation 4.9 – Closure force angle

The calculated closure force and angle values for each of the subjects that was used in the training set are shown in Table 4.2. Raw anatomical measurement data used to calculate the closure force and direction can be found in APPENDIX B. Detailed closure force and angle calculations data can be found in APPENDIX C.

Table 4.2 – Closure force and angle values

Subject code	Closure force (N)	Closure force angle (°)
2	1.21	-5.17
10	1.01	-0.94
20	0.97	-0.03
22	1.17	-1.12
31	1.29	-0.87
34	1.03	-1.38
37	1.08	-2.56
38	0.67	-3.15
41	0.83	-3.29
42	0.82	-2.29
Child002	0.65	-0.43
Child 005	0.68	-7.91
Child 006	0.79	-15.05
Child 004	0.83	-0.94
543	0.82	-0.43
400	0.69	-2.09
449	0.92	-2.31
448	0.97	-0.03
356	0.94	-1.51
324	0.75	-0.03

The calculated closure force and angle values along with their corresponding muscle dimensions were used to predict the closure force and angle values for unknown muscle dimensions in MATLAB [14]. The code used for prediction can be found in APPENDIX D. The class multi.m loads the training set data to predict closure force from closureForceData.txt and closure force angle from angleData.txt. The data is then normalized by calling the class featureNormalize.m. multi.m then calls normalEqn.m to predict the closure force and its corresponding angle is predicted using normal equations.

CHAPTER 5 – RESULTS

The program created in MATLAB (APPENDIX D) with the multiple linear regression algorithm that uses normal equations to calculate regression coefficients was able to successfully predict the closure force and angle values when it was run for any set of anatomical parameters input by the user upon being prompted by the program. Figure 5.1 shows the program being executed in MATLAB where it loads the training set data, normalizes them, calculates the regression coefficients based on the training set values, prompts the user to input anatomical parameters for prediction, and then predicts the closure force and its direction.

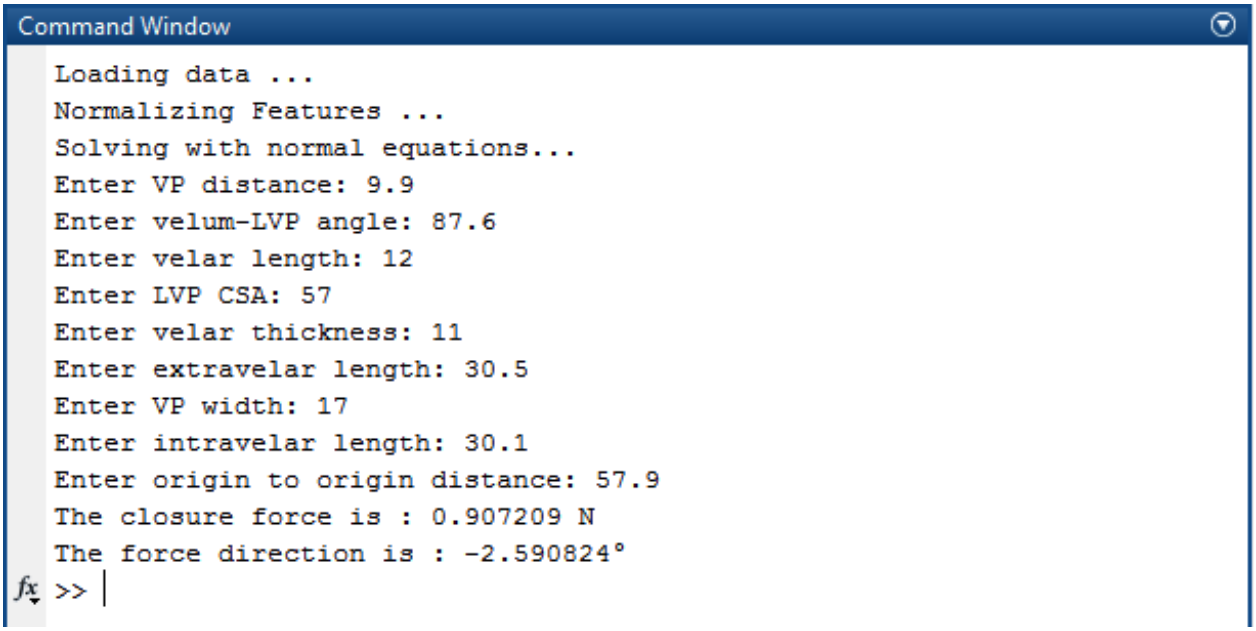

Figure 5.1 – Program execution in MATLAB

To validate the model, the training set's closure forces were checked for linearity, as it had been shown in previous studies that closure force increases linearly with increase in the muscle activation level [6, 32]. Figure 5.2 displays a graphical plot found in a computational modeling study [6] where closure force increases linearly with increase in muscle activation for average, individual and randomized models.

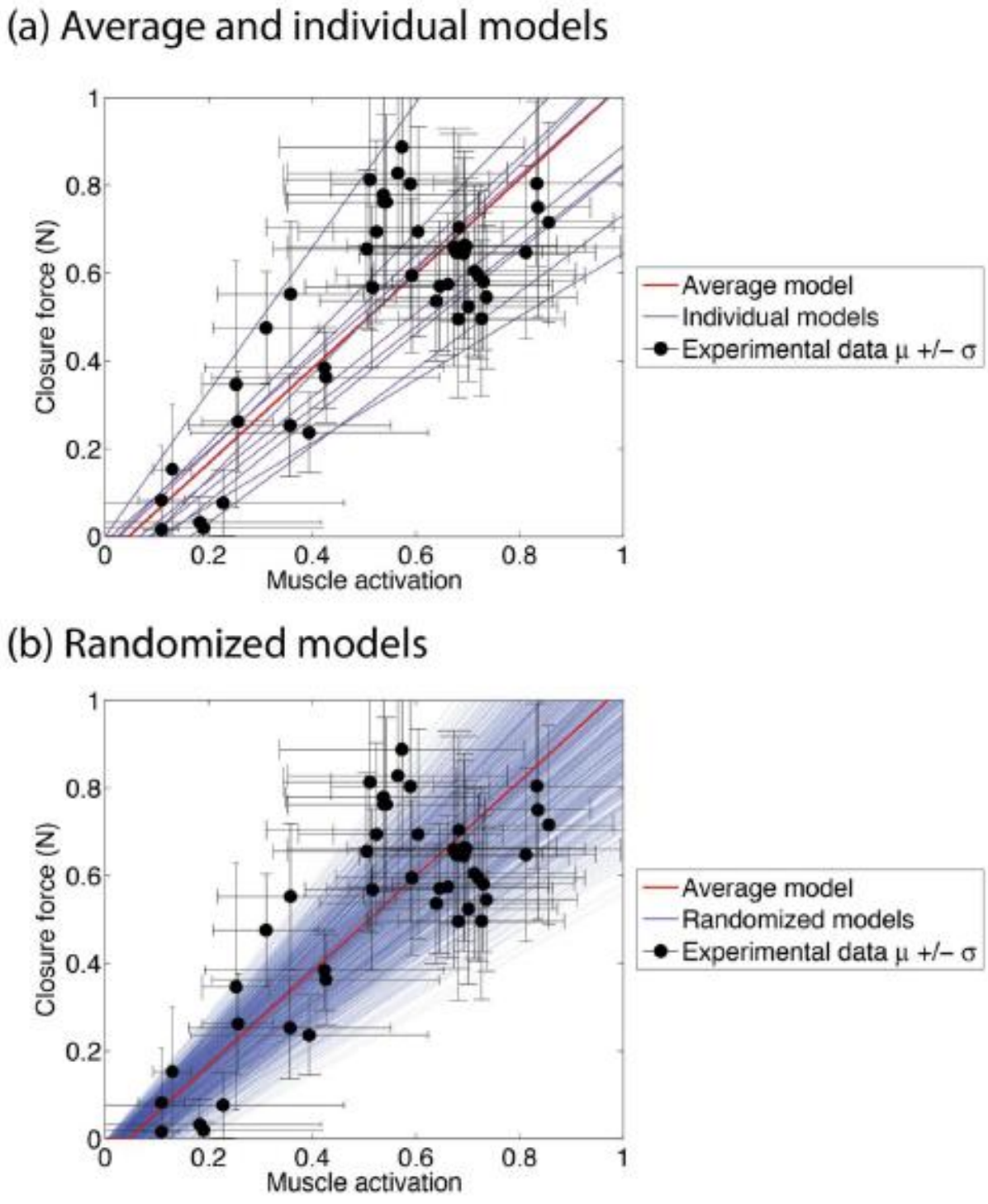

Figure 5.2 – Linearity of closure force in a modeling study [6]

Table 5.1 – Data from the force bulb study [32]

Closure Force (g)	Muscle Activation (%)
26.7	25.7
35.3	25.3
48.5	31.1
56.3	35.8
60.7	59.2
57.9	51.6
81.9	58.9
70.8	60.4
1.6	10.9
76.5	83.5
67.2	67.3
82.9	51.1
66.8	50.5
84.4	56.5
77.7	53.8
15.6	13.0
82	83.3
71.8	68.3
79.4	53.7
70.8	52.4
90.5	57.3
77.7	54.3
8.4	10.9

Similarly, data gathered from a study [32] that used a force bulb to calculate closure force values is plotted in Figure 5.3, which shows linear increase in closure force with increase in muscle activation level. Data from only male subjects was used as there are significant differences between males and females across several levator muscle measures [4] and males exhibit a higher velopharyngeal closure force than females [32]. Table 5.1 displays data gathered from the study.

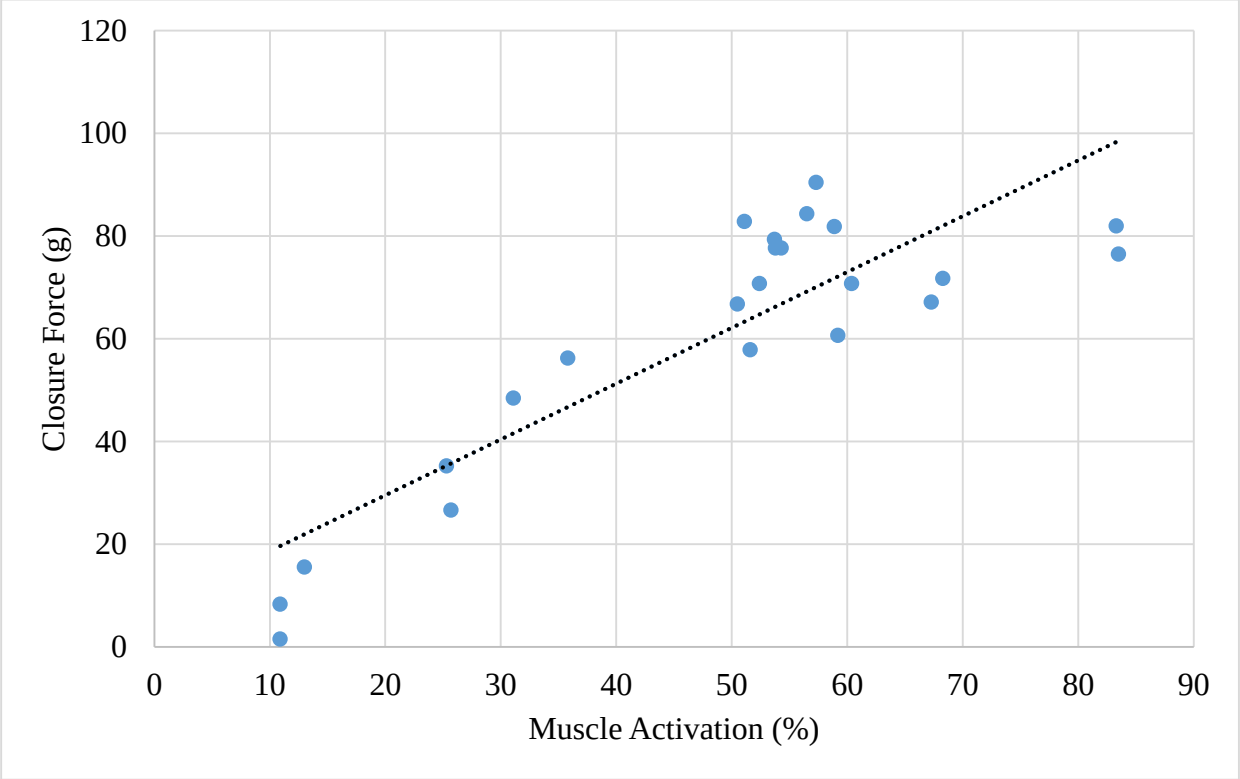

Figure 5.3 – Linearity of closure force in force bulb study

Additionally, having linearity is one of the conditions of linear regression analysis [7]. Therefore, it was important to establish linearity with the training set being used. To achieve this, closure force values were calculated for each of the subjects in the training set at various muscle activation levels, the raw data for which can be found in APPENDIX E.

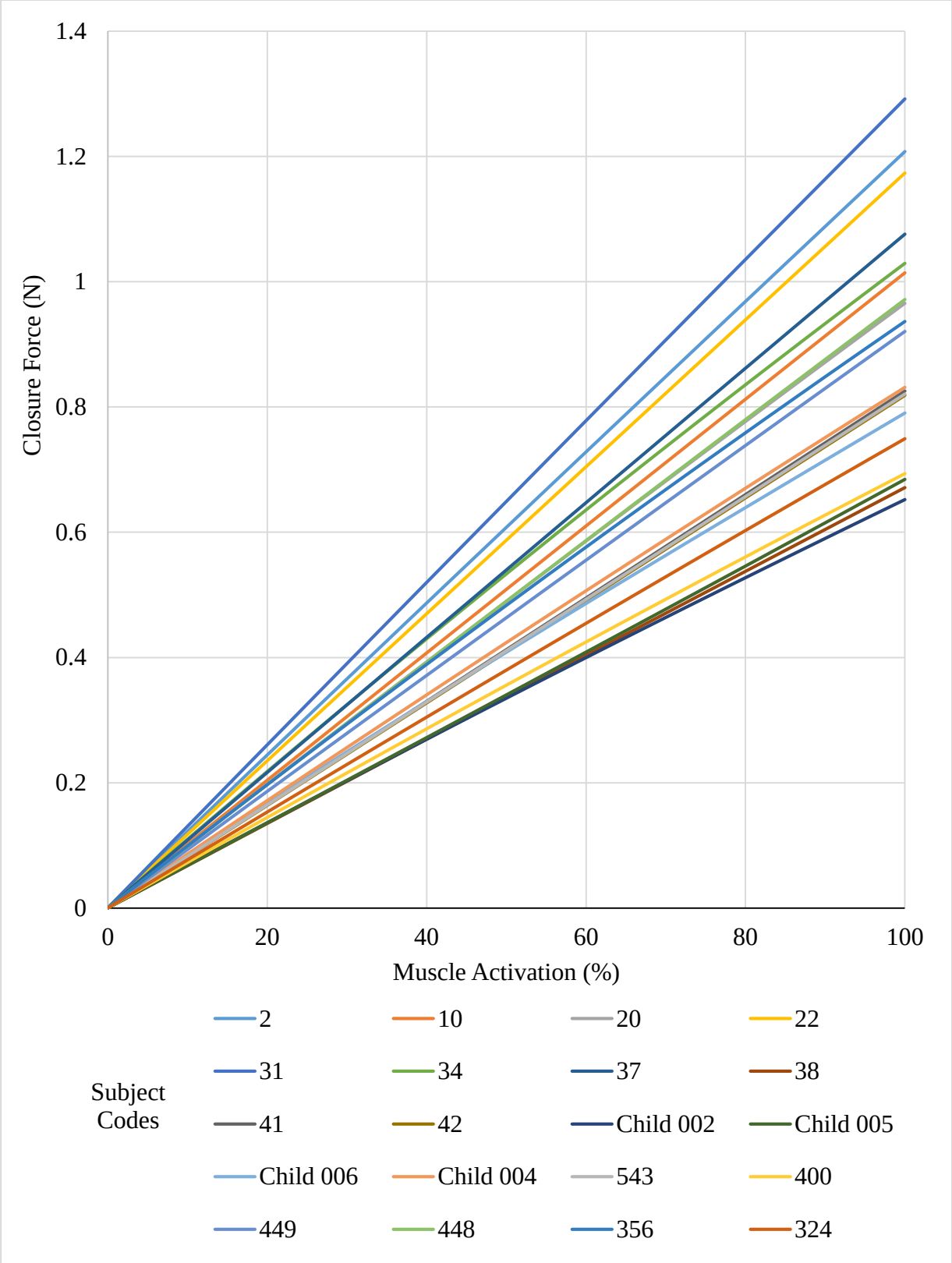

Figure 5.4 – Closure force linearity with multiple linear regression

Figure 5.4 shows that each of the subjects in the training set displayed a linear increase in closure force with increase in muscle activation level which suggests that the training set being used yields accurate results. Similar calculation was performed with closure force angles at varying muscle activation levels which showed that angles increase in the negative z-axis direction with increase in muscle activation level, displayed in Figure 5.5, the raw data for which can be found in APPENDIX F. This indicates that closure force acts in the downward direction on the posterior pharyngeal wall as it moves from rest to 100% activation, further validating the model.

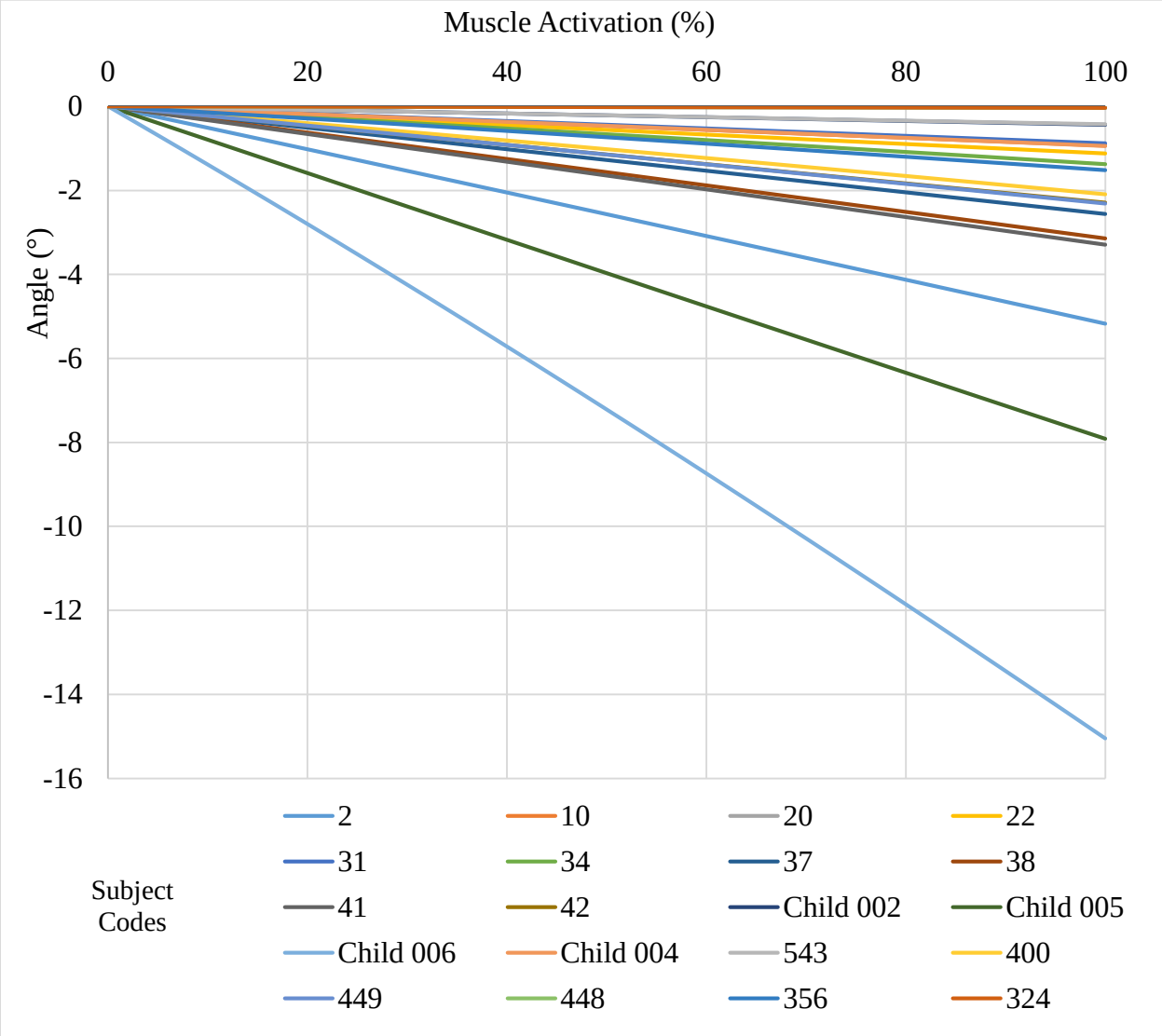

Figure 5.5 – Increase in closure force angle

CHAPTER 6 – DISCUSSION

After the training set's validation, it was possible to study the effects of velopharyngeal anatomical parameters on velopharyngeal closure force. For this purpose, new sets of muscle dimensions were generated where each of the muscle parameters was increased and decreased by one standard deviation for this average set. The outputs predicted from these sets using the multiple linear regression algorithm program in MATLAB (APPENDIX D) were used to analyze the effects of variability in velopharyngeal anatomy on velopharyngeal function. Table 6.1 shows the average values of each of the muscle parameters in the training set and their corresponding standard deviation. The change in closure force and its direction due to change in anatomical parameters are shown in Table 6.2 and Table 6.3, respectively. Their combined effect can be observed in Figure 6.1 and Figure 6.2.

Table 6.1 – Average anatomical parameter values

Anatomical Parameter	Average	Standard Deviation
VP Distance	9.9 mm	2.6 mm
Velum-LVP Angle	87.6°	12.6°
Velar Length	12 mm	2.5 mm
LVP CSA	57 mm2	21.9 mm2
Velar Thickness	11 mm	1.6 mm
Extravelar Length	30.5 mm	3.7 mm
VP Width	17 mm	2.9 mm
Intravelar Segment	30.1 mm	6 mm
Origin to Origin	57.9 mm	4.1 mm

Table 6.2 – Change in closure force due to change in anatomical parameters

Anatomical Parameter	High STD value	Closure Force	Change increase	Low STD value	Closure Force	Change decrease
VP Distance	12.48 mm	0.915 N	0.93%	7.22 mm	0.898 N	-0.95%
Velum-LVP Angle	100.13°	0.907 N	0.03%	75.00°	0.906 N	-0.03%
Velar Length	14.40 mm	0.924 N	1.92%	9.55 mm	0.889 N	-1.99%
LVP CSA	78.94 mm^2	0.890 N	-0.71%	35.10 mm^2	0.913 N	0.70%
Velar Thickness	12.59 mm	1.039 N	12.75%	9.37 mm	0.774 N	-17.11%
Extravelar Length	34.22 mm	0.891 N	-1.72%	26.74 mm	0.922 N	1.67%
VP Width	19.95 mm	1.050 N	13.67%	14.09 mm	0.763 N	-18.82%
Intravelar Segment	36.08 mm	0.900 N	-0.74%	24.06 mm	0.913 N	0.73%
Origin-Origin	62.00 mm	0.928 N	2.33%	53.87 mm	0.885 N	-2.44%

Table 6.3 – Change in angle due to change in anatomical parameters

Anatomical Parameter	High STD value	Angle (°)	Change increase	Low STD value	Angle (°)	Change decrease
VP Distance	12.48 mm	-3.11	17.27%	7.22 mm	-2.04	-26.38%
Velum-LVP Angle	100.13°	-4.63	44.34%	75.00°	-0.52	-391.69%
Velar Length	14.40 mm	-2.23	-15.73%	9.55 mm	-2.93	11.96%
LVP CSA	78.94 mm^2	-6.47	60.14%	35.10 mm^2	1.31	296.43%
Velar Thickness	12.59 mm	-1.25	-106.00%	9.37 mm	-3.90	33.97%
Extravelar Length	34.22 mm	-3.99	35.37%	26.74 mm	-1.17	-120.85%
VP Width	19.95 mm	-2.82	8.71%	14.09 mm	-2.33	-10.55%
Intravelar Segment	36.08 mm	-4.43	41.87%	24.06 mm	-0.72	-257.55%
Origin-Origin	62.00 mm	-1.48	-74.09%	53.87 mm	-3.67	29.85%

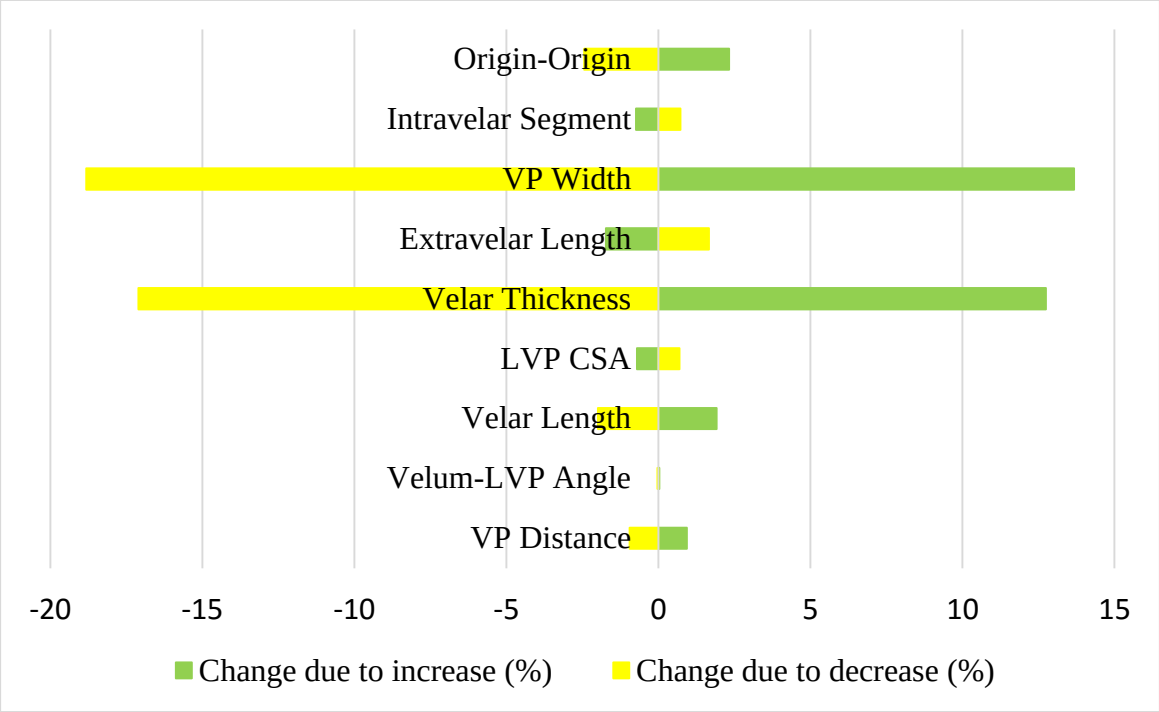

Figure 6.1 – Change in closure force due to change in anatomical parameters

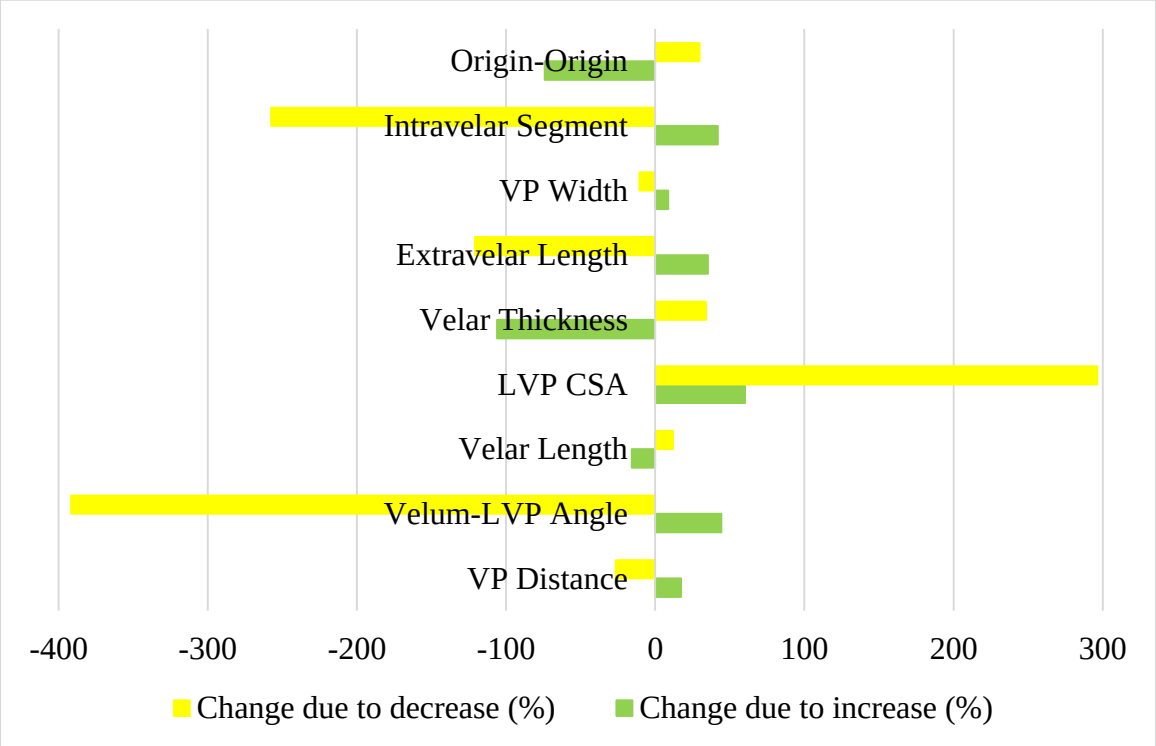

Figure 6.2 – Change in angle due to change in anatomical parameters

Velopharyngeal port width and velar thickness had the greatest influence on change in closure force. Increase in their length caused an increase in closure force and vice-versa. This is expected behavior. As mentioned in Equation 4.4, the cross sectional area of the velum is the algebraic product of velar thickness and velopharyngeal port width. Increase in cross sectional area of the velum causes an increase in the force generated by the velum, as explained in Equation 4.3, which in turn increases the closure force achieved. Conversely, the levator veli palatini muscle pulls the velum reducing the overall closure force generated. All the parameters related to the levator veli palatini muscle – the extravelar segment, the intravelar segment, and the levator veli palatini cross sectional area, cause a decrease in closure force when their dimensions are increased and vice-versa. This behavior is opposite to the influence displayed by the velopharyngeal port width and velar thickness. Therefore, the primary job of the levator veli palatini muscle is to aid the velopharyngeal system in moving the velum rather than generating significant force. The other anatomical parameters do not significantly influence closure force.

These results are in contradiction with previous studies which suggest that the levator veli palatini muscle and the velopharyngeal port distance are major influencers of closure force compared to the velum [6, 10]. To further investigate this contradiction, the velum cross sectional area (velopharyngeal port width and velar thickness) and combined levator veli palatini muscles (extravelar segment, intravelar segment, and the levator veli palatini cross-sectional area) were increased and decreased by one standard deviation and run through the algorithm separately to gauge their influence on closure force, as shown in Table 6.4 and Figure 6.3. It can be seen that the velum cross sectional area has a greater influence on closure force compared to the levator veli palatini muscles. Also, the latter's influence is opposite adding further proof to the observation in Figure 6.1.

Table 6.4 – Closure force change due to velum CSA and LVP muscles

Anatomical Parameter	High STD Closure Force	Change due to increase	Low STD Closure Force	Change due to decrease
Velum CSA	1.1821 N	23.34%	0.6303 N	-43.77%
LVP muscles	0.8778 N	-3.23%	0.9346 N	3.04%

Table 6.5 – Angle change due to velum CSA and LVP muscles

Anatomical Parameter	High STD Angle	Change due to increase	Low STD Angle	Change due to decrease
Velum CSA	-1.50°	-72.16%	-3.66°	29.53%
LVP muscles	-9.73°	73.52%	4.58°	156.29%

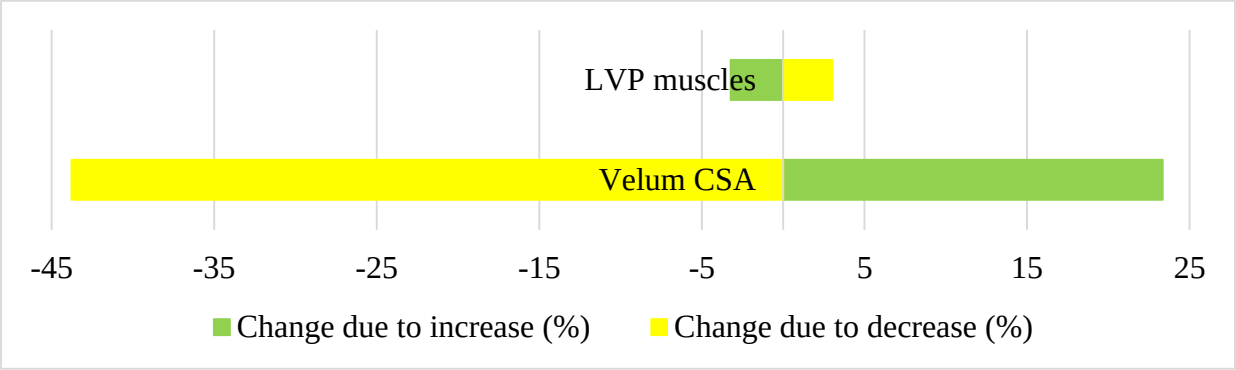

Figure 6.3 – Closure force change due to velum CSA and LVP muscles

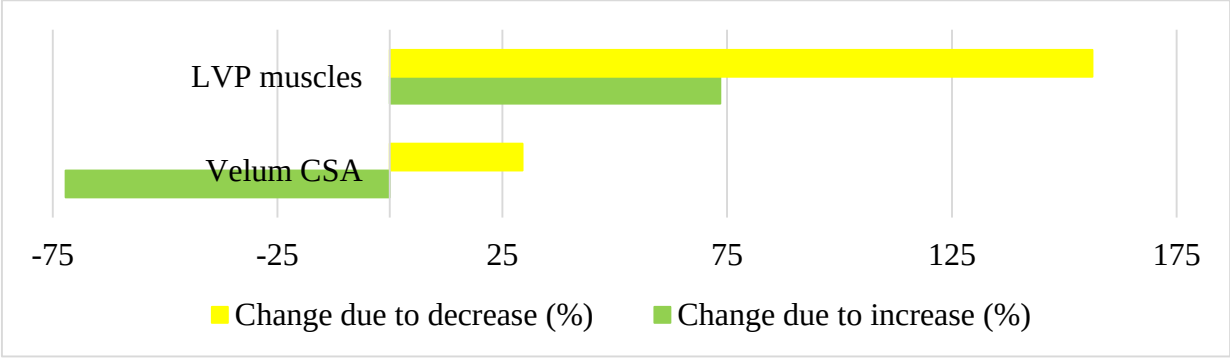

Figure 6.4 – Angle change due to velum CSA and LVP muscles

Contrary to the case of closure force, the levator veli palatini muscle has a greater influence on the direction of closure force than the other anatomical parameters. As can be seen in Figure 6.2, the levator veli palatini cross sectional area, the extravelar segment, the intravelar segment and the angle the levator veli palatini muscle makes with the velum have a significant effect on the direction of closure force. Figure 6.4 also shows that there is a greater change in the direction of closure force when the levator veli palatini muscle's dimensions are changed compared to the cross sectional area of the velum. This adds further support to the argument that the levator veli palatini muscle acts as a support structure that maintains direction rather than generating the bulk of the force as was evident in Figure 6.1 and Figure 6.3, where it did not have a significant effect on closure force compared to the cross sectional area of the velum. However, the influence seems to be a combined effort with other anatomical parameters rather than the muscle itself because the changes observed in Figure 6.2 and Figure 6.4 are not symmetrical, unlike the effect on closure force. This is especially true for the cross sectional area of the levator veli palatini muscle which indicates a significant influence on closure force direction but decreasing or increasing its parameters only causes an increase in the change but never cause a decrease. These findings are supported by a finite element modeling study [10] which states that the distance between the velum and the posterior pharyngeal wall decreases linearly with an increase in the velar force exponentially, and that the soft palate continues moving upwards along the posterior pharyngeal wall after initial contact, thereby producing a reactionary downward force.

A patient's ability to generate a high closure force is necessary to overcome velopharyngeal inadequacy, as a higher closure force ensures that the velum is pressed against the posterior pharyngeal wall, creating a tight seal necessary for speech production. This study focused on measuring the variability in velopharyngeal anatomical parameters on velopharyngeal function.

However, in order to gauge the effectiveness of this model, future studies should use data from patients with abnormal velopharyngeal anatomy. Also, this study used a select few anatomical parameters but it is necessary to include craniometrics. This is because the velum and the levator veli palatini muscle experience reaction forces being generated due to the movement of the cranium. Therefore, including this information will allow the discovery of parameters that are ultimately responsible for regulating closure force. One addition that could significantly influence the study is the musculus uvulae. This muscle is an intrinsic part of the velopharyngeal system that adds stiffness and aids in filling the velopharyngeal gap by providing muscle bulk [38]. The musculus uvulae will act as a load bearing structure that could influence closure force, for which reason future studies should to include it in their models.

CHAPTER 7 – CONCLUSION

Computational modeling in combination with magnetic resonance imaging has been a popular method in recent times for investigating velopharyngeal anatomy. However, this process is expensive and impractical. Reliable computational modeling software costs thousands of dollars and require technical expertise to be an effective tool. To tackle this issue, this study introduced a machine learning algorithm, multiple linear regression, which can be as effective as computational modeling in investigating velopharyngeal anatomy while allowing researchers with little technical expertise to use it.

One of the key areas where multiple linear regression, or linear regression in general, is advantageous over computational modeling is that they are entirely data driven and self-learning. In computational modeling, the relationship and functionality is provided whereas in machine learning, the system is capable of forming relations based on historic data. While some of these relations are obvious, such as the usage of similar demographic subjects, others are unknown either due to lack of information or accessibility to the technology required. Also, machine learning algorithms such as linear regression perform better with increase in the data provided [30]. Therefore, models can continually be updated with the latest data allowing its prediction capabilities to get better.

The failure rate of first time cleft palate repairs is 25-35% [39]. The model can help speech pathologists, surgeons, related professionals and researchers gauge the effect of velopharyngeal muscles to reduce this failure rate and prevent the need for further surgeries. This model was implemented using MATLAB. This is an expensive software not within the means of every individual or organization. However, the multiple linear regression algorithm can easily be implemented in other languages or by using other tools. Also, the code provided (APPENDIX D)

can be implemented as it is in Octave [40] which is a high level interpreted open source language that is available free of charge. Creating a user interface and shipping the program with the algorithm as an executable file will make it accessible to a larger user base.

The potential for this algorithm shipped as a software is huge and will advance the quest towards effectively treating children with a cleft lip and palate.

REFERENCES

[1] E. A. Martin and T. A. McFerran, A Dictionary of Nursing (6 ed.), Oxford University Press, 2014.

[2] J. L. Perry, "Anatomy and Physiology of the Velopharyngeal Mechanism," *Seminars in Speech and Language*, vol. 32, no. 2, pp. 83-92, 2011.

[3] J. L. Perry, "Studying the Velopharyngeal Mechanism Through 3D Computer Reconstructions Based on Magnetic Resonance Imaging," *Journal of Oral and Maxillofacial Surgery*, vol. 64, no. 9, pp. 88-89, 2006.

[4] J. L. Perry, D. P. Kuehn, B. P. Sutton and J. K. Gamage, "Sexual Dimorphism of the Levator Veli Palatini Muscle: An Imaging Study," *The Cleft Palate - Craniofacial Journal*, pp. 544-552, 2014.

[5] J. L. Perry, D. P. Kuehn and B. P. Sutton, "Morphology of the levator veli palatini muscle using magnetic resonance imaging," *Cleft Palate-Craniofacial Journal*, vol. 50, no. 1, pp. 64-75, 2013.

[6] J. M. Inouye, J. L. Perry, K. Y. Lin and S. S. Blemker, "A Computational Model Quantifies the Effect of Anatomical Variability on Velopharyngeal Function," *Journal of speech, language, and hearing research*, vol. 58, no. 4, pp. 1119-1133, 2015.

[7] X. Yan, Linear Regression Analysis : Theory and Computing, World Scientific, 2009, p. 2.

[8] A. Sana, J. L. Perry and N. Tabrizi, "A Review of Image Segmentation Techniques for Tracking the Velum," in *International Conference on Computational Science and Computational Intelligence*, Las Vegas, 2015.

[9] A. Sana, J. L. Perry and N. Tabrizi, "Investigating Velopharyngeal Closure Force with Linear Regression," in *IEEE International Conference on Biomedical and Health Informatics*, Las Vegas, 2016.

[10] D. A. Berry, J. B. Moon and D. P. Kuehn, "A finite element model of the soft palate," *The Cleft Palate - Craniofacial Journal*, vol. 36, no. 3, pp. 217-223, 1999.

[11] Dassault Systèmes, "ABAQUS UNIFIED FEA," Dassault Systèmes, 2002-2015. [Online]. Available: http://www.3ds.com/products-services/simulia/products/abaqus/. [Accessed 11 November 2015].

[12] P. Rong, "Using articulatory adjustment to compensate for hypernasality ? a modeling study based on measures of electromagnetic articulography (EMA)," ProQuest Dissertations Publishing, Ann Arbor, 2012.

[13] P. Rahimian, "Using synchronized audio mapping to predict velar and pharyngeal wall locations during dynamic MRI sequences," East Carolina University, Greenville, 2013.

[14] MathWorks, "The Language of Technical Computing," The MathWorks, Inc., 1994-2015. [Online]. Available: http://www.mathworks.com/products/matlab/. [Accessed 11 November 2015].

[15] A. Alwan, "Modeling speech production and perception mechanisms and their applications to synthesis, recognition, and coding," in *Proceedings of the Fifth International Symposium on Signal Processing and its Applications*, Brisbane, 1999.

[16] A. Serrurier and P. Badin, "Towards a 3D articulatory model of velum based on MRI and CT images," *ZAS Papers in Linguistics (Speech production and perception: Experimental analyses and models),* vol. 40, pp. 195-211, 2005.

[17] Autodesk, "MAYA," Autodesk Inc., 2015. [Online]. Available: http://www.autodesk.com/products/maya/overview-dts?s_tnt=69290:1:0. [Accessed 11 November 2015].

[18] J. L. Perry and D. P. Kuehn, "Three-dimensional computer reconstruction of the levator veli palatini muscle in situ using magnetic resonance imaging," *The Cleft palate-craniofacial journal,* vol. 44, no. 4, pp. 421-423, 2007.

[19] J. L. Perry and D. P. Kuehn, "Magnetic resonance imaging and computer reconstruction of the velopharyngeal mechanism," *Journal of Craniofacial Surgery,* vol. 20, no. 8, pp. 1739-1746, 2009.

[20] R. Grycuk, M. Gabryel, M. Korytkowski, R. Scherer and S. Voloshynovskiy, "From Single Image to List of Objects Based on Edge and Blob Detection," in *Artificial Intelligence and Soft Computing*, Zakopane, Springer International Publishing, 2014, pp. 605-615.

[21] P. Sujatha and K. K. Sudha, "Performance Analysis of Different Edge Detection Techniques for Image Segmentation," *Indian Journal of Science and Technology,* vol. 8, no. 14, pp. 1-6, 2015.

[22] Video/Image Modeling and Synthesis Lab, "EdgeTrak System," University of Delaware, 26 April 2012. [Online]. Available:

https://www.eecis.udel.edu/wiki/vims/index.php/Main/EdgeTrak. [Accessed 9 September 2015].

[23] Z. Ghahramani, "An Introduction to Hidden Markov Models and Bayesian Networks," *International Journal of Pattern Recognition & Artificial Intelligence,* vol. 15, no. 1, pp. 9 - 42, 2001.

[24] M. Li, C. Kambhamettu and M. Stone, "Automatic contour tracking in ultrasound images," *Clinical Linguistics & Phonetics,* vol. 19, no. 6-7, pp. 545-554, 2005.

[25] "About Blender," [Online]. Available: http://www.blender.org/manual/getting_started/about_blender/index.html. [Accessed August 31 2015].

[26] Video/Image Modeling and Synthesis Lab, "EdgeTrak System," 25 April 2012. [Online]. Available: http://vims.cis.udel.edu/EdgeTrak/EdgeTrak_V2.tar. [Accessed 26 April 2015].

[27] H. Ardo, K. Astrom and R. Berthilsson, "Real Time Viterbi Optimization of Hidden Markov Models for Multi Target Tracking," in *Motion and Video Computing, 2007. WMVC '07. IEEE Workshop on*, Austin, 2007.

[28] X. Xie and R. Evans, "Multiple target tracking using hidden Markov models," in *Radar Conference, 1990., Record of the IEEE 1990 International*, Arlington, 1990.

[29] J. Gai, Y. Li and R. Stevenson, "Coupled Hidden Markov Models for Robust EO/IR Target Tracking," in *Image Processing, 2007. ICIP 2007. IEEE International Conference on (Volume:1)*, San Antonio, 2007.

[30] M. Banko and E. Brill, "Scaling to very very large corpora for natural language disambiguation," in *ACL '01 Proceedings of the 39th Annual Meeting on Association for Computational Linguistics*, Stroudsburg, 2001.

[31] S. Lefevre, E. Bouton, T. Brouard and N. Vincent, "A new way to use hidden Markov models for object tracking in video sequences," in *Image Processing, 2003. ICIP 2003. Proceedings. 2003 International Conference on (Volume:3)*, 2003.

[32] D. P. Kuehn and J. B. Moon, "Velopharyngeal closure force and levator veli palatini activation levels in varying phonetic contexts," *Journal of Speech, Language, and Hearing Research,* vol. 41, no. 1, pp. 51-62, 1998.

[33] S. Cheng, S. Gandevia, M. Green, R. Sinkus and L. Bilston, "Viscoelastic properties of the tongue and soft palate using MR elastography," *Journal of Biomechanics,* vol. 44, no. 3, pp. 450-454, 2011.

[34] L. Huang, "Mechanical modeling of palatal snoring," *The Journal of the Acoustical Society of America,* vol. 97, no. 6, pp. 3642-3648, 1995.

[35] M. H. Huang, J. E. Riski, S. R. Cohen, C. A. Simms and B. F. D, "An anatomic evaluation of the furlow double opposing Z-plasty technique of cleft palate repair," *Annals of the Academy of Medicine, Singapore,* vol. 28, no. 5, pp. 672-676, 1999.

[36] Z. Liu, X. Luo, H. Lee and C. Lu, "Snoring source identification and snoring noise prediction," *Journal of Biomechanics,* vol. 40, no. 4, pp. 861-870, 2007.

[37] A. Malhotra, Y. Huang, R. B. Fogel, G. Pillar, J. K. Edwards, R. Kikinis, S. H. Loring and D. P. White, "The Male Predisposition to Pharyngeal Collapse: Importance of Airway Length," *American Journal of Respiratory and Critical Care Medicine,* vol. 166, no. 10, pp. 1388-1395, 2002.

[38] M. H. Huang, S. T. Lee and K. Rajendran, "Structure of the musculus uvulae: functional and surgical implications of an anatomic study.," *The Cleft Palate-Craniofacial Journal,* vol. 34, no. 6, pp. 466-474, 1997.

[39] B. J. McWilliams, "The long-term speech results of primary and secondary surgical correction of palatal clefts.," in *Multidisciplinary Management of Cleft Lip and Palate.*, Philadelphia, WB Saunders, 1990, pp. 815-819.

[40] J. W. Eaton, "GNU Octave," 29 May 2015. [Online]. Available: https://www.gnu.org/software/octave/. [Accessed 17 November 2015].

APPENDIX A – SUBJECT DEMOGRAPHICS

Subject code	Age at scan	Height	Weight (lb.)	Gender (1=M; 2=F)	Race (1=Caucasian; 2=African American; 3=Asian; 4=Hispanic; 5=Interracial
2	22	5'10"	165	1	1
10	21	6'2"	170	1	1
20	20	5'7"	170	1	1
22	20	5'11"	140	1	1
31	20	6'1"	185	1	1
34	22	5'11"	183	1	1
37	22	5'5"	170	1	1
38	20	5'11"	170	1	1
41	22	5'6"	150	1	1
42	19	5'9"	160	1	1
Child002	5	4'2"	50	1	1
Child 005	6	4'2"	50	1	1
Child 006	5	4'	45	1	1
Child 004	9	5'	60	1	1
543	8			1	1
400	8			1	1
449	9			1	1
448	9			1	1
356	9			1	1
324	9			1	1

APPENDIX B – RAW ANATOMICAL MEASUREMENTS

Subject (mm)	VP Distance (mm)	Velum -LVP Angle (°)	Velar Length (mm)	LVP CSA (mm^2)	Velar Thickness at Mid LVP (mm)	Extravelar Length (mm)	VP Width (mm)	Intravelar Segment (mm)	O-O (mm)
2	10.005	74.3	11.8	84.004	13.66	30.48	17.94	36.16	62.79
10	12.895	83.9	12.71	33.36	11.03	31.54	18.5	40.02	58.6
20	9.215	88.3	13.35	44.286	11.61	33.9	17.1	29.15	58.12
22	16.705	80.4	13.21	39.138	12.51	33.21	18.79	31.22	57.88
31	7.68	70.2	16.95	61.516	11.63	39.28	22.43	36.18	70.85
34	11.555	78.4	13.58	70.47	13.58	34.59	16.26	36.36	60.04
37	13.765	77.4	14.59	55.839	9.78	29.23	22.15	33.27	58.5
38	6.955	80.5	12.25	49.016	10.71	29.14	12.62	37.87	52.38
41	10.47	77.1	11.34	58.659	13.68	31.1	12.06	40.02	55.25
42	10.775	73.7	16.19	55.540	11.68	34.53	14.02	32.43	58.83
Child 002	9.865	73	12.7	65.056	9.08	24.045	15.14	28.3	52.97
Child 005	9.53	95.7	13.61	93.650	10.1	30.025	13.46	22.88	56.07
Child 006	5.855	109.1	10.69	119.07	11.12	26.955	15.42	22.7	53.52
Child 004	11.695	84.6	8.22	46.906	9.62	33.595	17.95	23.35	59.51
543	10.31	93.3	9.74	20.141	7.59	31.865	21.68	25.13	57.84
400	8.58	90.7	10.33	52.984	9.64	28.765	15.14	27.55	56.11
449	10.03	99.6	10.54	49.821	9.51	25.555	19.63	24.46	53.5
448	8.705	107.1	10.32	33.243	10.73	30.29	18.4	26.7	61.55
356	6.49	106.6	6.63	63.823	12.47	27.735	15.98	20.2	55.11
324	5.97	107.4	10.78	43.913	9.81	23.805	15.7	27.46	59.33

APPENDIX C – DETAILED CLOSURE FORCE CALCULATION

Subject Code	F_v (N)	F_{lvp} (N)	F_{lvpx} (+/-N)	F_{lvpy} (+/-N)	F_{lvpz} (+/-N)	Σ y-axis (N)	Σ z-axis (N)	F_c (N)	F° (°)
2	1.225	-0.32988	0.19568	0.329873	0.15016	-0.10882	1.202755	1.207668	-5.16962
10	1.020	-0.131	0.08311	0.12881	0.079052	-0.01659	1.014026	1.014162	-0.93746
20	0.993	-0.17391	0.07477	0.022407	0.16422	-0.0005	0.965687	0.965687	-0.02979
22	1.175	-0.1537	0.07224	0.151343	0.04386	-0.0229	1.173391	1.173614	-1.11827
31	1.304	-0.24157	0.11125	0.14043	0.1128	-0.01972	1.29158	1.291731	-0.87477
34	1.104	-0.27674	0.14545	0.15727	0.274035	-0.02473	1.028959	1.029256	-1.37692
37	1.083	-0.21928	0.12479	0.21916	0.091607	-0.04803	1.074743	1.075816	-2.5588
38	0.676	-0.19249	0.12508	0.191941	0.07307	-0.03684	0.670462	0.671473	-3.1452
41	0.825	-0.23035	0.14821	0.21765	0.030085	-0.04737	0.823999	0.825359	-3.2903
42	0.819	-0.2181	0.10242	0.180983	0.027717	-0.03275	0.818	0.818655	-2.29305
Child 002	0.687	-0.25547	0.15034	0.070297	0.188078	-0.00494	0.651983	0.652001	-0.43426
Child 005	0.680	-0.36776	0.14012	0.30697	0.04351	-0.09423	0.677837	0.684356	-7.91459
Child 006	0.857	-0.46759	0.19689	0.453	0.306579	-0.20521	0.763361	0.790463	-15.0469
Child 004	0.863	-0.1842	0.06401	0.11691	0.179637	-0.01367	0.831126	0.831238	-0.94214
543	0.823	-0.07909	0.03119	0.078101	0.04615	-0.0061	0.820626	0.820649	-0.42588
400	0.730	-0.20807	0.09964	0.15914	0.191139	-0.02533	0.693214	0.693676	-2.09227
449	0.933	-0.19565	0.09363	0.192652	0.11681	-0.03711	0.919761	0.92051	-2.31077
448	0.987	-0.13055	0.05754	0.023212	0.12525	-0.00054	0.971473	0.971473	-0.03178
356	0.996	-0.25063	0.09127	0.157354	0.24491	-0.02476	0.936373	0.9367	-1.51471
324	0.770	-0.17244	0.09946	0.02086	0.14369	-0.00043	0.749439	0.749439	-0.03325

APPENDIX D – CODE

multi.m

```
%% Clear and Close Figures
clear ; close all; clc

fprintf('Loading data ...\n');

%% Load Data
data = load('closureForceData.txt');
X = data(:, 1:9);
y = data(:, 10);
m = length(y);

dataa = load('angleData.txt');
Xa = dataa(:, 1:9);
ya = dataa(:, 10);
ma = length(ya);

% Scale features and set them to zero mean
fprintf('Normalizing Features ...\n');

[X mu sigma] = featureNormalize(X);
[Xa mu sigma] = featureNormalize(Xa);

% Add intercept term to X
X = [ones(m, 1) X];
Xa = [ones(ma, 1) Xa];

fprintf('Solving with normal equations...\n');

%% Load Data
data = csvread('closureForceData.txt');
X = data(:, 1:9);
y = data(:, 10);
m = length(y);

dataa = csvread('angleData.txt');
Xa = dataa(:, 1:9);
ya = dataa(:, 10);
ma = length(ya);

% Add intercept term to X
X = [ones(m, 1) X];
Xa = [ones(ma, 1) Xa];
```

```
% Calculate the parameters from the normal equation
theta = normalEqn(X, y);
thetaa = normalEqn(Xa, ya);

% Calculate closure force
d = [];
d(1) = 1;
prompt2 = 'Enter VP distance: ';
d(2) = input(prompt2);
prompt3 = 'Enter velum-LVP angle: ';
d(3) = input(prompt3);
prompt4 = 'Enter velar length: ';
d(4) = input(prompt4);
prompt5 = 'Enter LVP CSA: ';
d(5) = input(prompt5);
prompt6 = 'Enter velar thickness: ';
d(6) = input(prompt6);
prompt7 = 'Enter extravelar length: ';
d(7) = input(prompt7);
prompt8 = 'Enter VP width: ';
d(8) = input(prompt8);
prompt9 = 'Enter intravelar length: ';
d(9) = input(prompt9);
prompt10 = 'Enter origin to origin distance: ';
d(10) = input(prompt10);
closureforce = d * theta;
angle = d * thetaa;

fprintf('The closure force is : %f N\n', closureforce);

fprintf('The force direction is : %f°\n', angle);
```

featureNormalize.m

```
function [X_norm, mu, sigma] = featureNormalize(X)

X_norm = X;
mu = zeros(1, size(X, 2));
sigma = zeros(1, size(X, 2));

mu = mean(X_norm);
sigma = std(X_norm);

tf_mu = X_norm - repmat(mu,length(X_norm),1);
tf_std = repmat(sigma,length(X_norm),1);

X_norm = tf_mu ./ tf_std;

end
```

normalEqn.m

```
function [theta] = normalEqn(X, y)

theta = zeros(size(X, 2), 1);

theta = pinv(X'*X)*X'*y;

end
```

closureForceData.txt

10.005, 74.3, 11.8, 84.0042, 13.66, 30.48, 17.94, 36.16, 62.79, 1.207667603

12.895, 83.9, 12.71, 33.36, 11.03, 31.54, 18.5, 40.02, 58.6, 1.014161542

9.215, 88.3, 13.35, 44.286, 11.61, 33.9, 17.1, 29.15, 58.12, 0.965686967

16.705, 80.4, 13.21, 39.1384, 12.51, 33.21, 18.79, 31.22, 57.88, 1.173614371

7.68, 70.2, 16.95, 61.5158, 11.63, 39.28, 22.43, 36.18, 70.85, 1.291730932

11.555, 78.4, 13.58, 70.47, 13.58, 34.59, 16.26, 36.36, 60.04, 1.029256261

13.765, 77.4, 14.59, 55.8392, 9.78, 29.23, 22.15, 33.27, 58.5, 1.075815869

6.955, 80.5, 12.25, 49.016, 10.71, 29.14, 12.62, 37.87, 52.38, 0.671472978

10.47, 77.1, 11.34, 58.6585, 13.68, 31.1, 12.06, 40.02, 55.25, 0.825359441

10.775, 73.7, 16.19, 55.5395, 11.68, 34.53, 14.02, 32.43, 58.83, 0.818655295

9.865, 73, 12.7, 65.0558, 9.08, 24.045, 15.14, 28.3, 52.97, 0.652001486

9.53, 95.7, 13.61, 93.6496, 10.1, 30.025, 13.46, 22.88, 56.07, 0.684356148

5.855, 109.1, 10.69, 119.071, 11.12, 26.955, 15.42, 22.7, 53.52, 0.790463094

11.695, 84.6, 8.22, 46.9056, 9.62, 33.595, 17.95, 23.35, 59.51, 0.831238011

10.31, 93.3, 9.74, 20.1405, 7.59, 31.865, 21.68, 25.13, 57.84, 0.820648944

8.58, 90.7, 10.33, 52.9842, 9.64, 28.765, 15.14, 27.55, 56.11, 0.693676422

10.03, 99.6, 10.54, 49.8212, 9.51, 25.555, 19.63, 24.46, 53.5, 0.920509688

8.705, 107.1, 10.32, 33.2431, 10.73, 30.29, 18.4, 26.7, 61.55, 0.971473055

6.49, 106.6, 6.63, 63.8232, 12.47, 27.735, 15.98, 20.2, 55.11, 0.936700387

5.97, 107.4, 10.78, 43.9125, 9.81, 23.805, 15.7, 27.46, 59.33, 0.749438982

angleData.txt

10.005, 74.3, 11.8, 84.0042, 13.66, 30.48, 17.94, 36.16, 62.79,-5.169622918

12.895, 83.9, 12.71, 33.36, 11.03, 31.54, 18.5, 40.02, 58.6,-0.937456071

9.215, 88.3, 13.35, 44.286, 11.61, 33.9, 17.1, 29.15, 58.12,-0.029790013

16.705, 80.4, 13.21, 39.1384, 12.51, 33.21, 18.79, 31.22, 57.88,-1.118273045

7.68, 70.2, 16.95, 61.5158, 11.63, 39.28, 22.43, 36.18, 70.85,-0.874769851

11.555, 78.4, 13.58, 70.47, 13.58, 34.59, 16.26, 36.36, 60.04,-1.376919959

13.765, 77.4, 14.59, 55.8392, 9.78, 29.23, 22.15, 33.27, 58.5,-2.558797721

6.955, 80.5, 12.25, 49.016, 10.71, 29.14, 12.62, 37.87, 52.38,-3.145198219

10.47, 77.1, 11.34, 58.6585, 13.68, 31.1, 12.06, 40.02, 55.25,-3.290295311

10.775, 73.7, 16.19, 55.5395, 11.68, 34.53, 14.02, 32.43, 58.83,-2.293053205

9.865, 73, 12.7, 65.0558, 9.08, 24.045, 15.14, 28.3, 52.97,-0.43426133

9.53, 95.7, 13.61, 93.6496, 10.1, 30.025, 13.46, 22.88, 56.07,-7.914586971

5.855, 109.1, 10.69, 119.071, 11.12, 26.955, 15.42, 22.7, 53.52,-15.04689466

11.695, 84.6, 8.22, 46.9056, 9.62, 33.595, 17.95, 23.35, 59.51,-0.942135176

10.31, 93.3, 9.74, 20.1405, 7.59, 31.865, 21.68, 25.13, 57.84,-0.425878679

8.58, 90.7, 10.33, 52.9842, 9.64, 28.765, 15.14, 27.55, 56.11,-2.092273378

10.03, 99.6, 10.54, 49.8212, 9.51, 25.555, 19.63, 24.46, 53.5,-2.310773145

8.705, 107.1, 10.32, 33.2431, 10.73, 30.29, 18.4, 26.7, 61.55,-0.031777705

6.49, 106.6, 6.63, 63.8232, 12.47, 27.735, 15.98, 20.2, 55.11,-1.514714748

5.97, 107.4, 10.78, 43.9125, 9.81, 23.805, 15.7, 27.46, 59.33,-0.033254334

APPENDIX E – CLOSURE FORCE AT VARYING ACTIVATION LEVELS

The closure forces are given in Newton and muscle activation levels are in %.

Subject	0	5	10	15	20	25	30	35	40	45	50	55	60	65	70	75	80	85	90	95	100
2	0	0.1	0.1	0.2	0.2	0.3	0.4	0.4	0.5	0.5	0.6	0.7	0.7	0.8	0.8	0.9	1.0	1.0	1.1	1.1	1.2
10	0	0.1	0.1	0.2	0.2	0.3	0.3	0.4	0.4	0.5	0.5	0.6	0.6	0.7	0.7	0.8	0.8	0.9	0.9	1.0	1.0
20	0	0.0	0.1	0.1	0.2	0.2	0.3	0.3	0.4	0.4	0.5	0.5	0.6	0.6	0.7	0.7	0.8	0.8	0.9	0.9	1.0
22	0	0.1	0.1	0.2	0.2	0.3	0.4	0.4	0.5	0.5	0.6	0.6	0.7	0.8	0.8	0.9	0.9	1.0	1.1	1.1	1.2
31	0	0.1	0.1	0.2	0.3	0.3	0.4	0.5	0.5	0.6	0.6	0.7	0.8	0.8	0.9	1.0	1.0	1.1	1.2	1.2	1.3
34	0	0.1	0.1	0.2	0.2	0.3	0.3	0.4	0.4	0.5	0.5	0.6	0.6	0.7	0.7	0.8	0.8	0.9	0.9	1.0	1.0
37	0	0.1	0.1	0.2	0.2	0.3	0.3	0.4	0.4	0.5	0.5	0.6	0.6	0.7	0.8	0.8	0.9	0.9	1.0	1.0	1.1
38	0	0.0	0.1	0.1	0.1	0.2	0.2	0.2	0.3	0.3	0.3	0.4	0.4	0.4	0.5	0.5	0.5	0.6	0.6	0.6	0.7
41	0	0.0	0.1	0.1	0.2	0.2	0.2	0.3	0.3	0.4	0.4	0.5	0.5	0.5	0.6	0.6	0.7	0.7	0.7	0.8	0.8
42	0	0.0	0.1	0.1	0.2	0.2	0.2	0.3	0.3	0.4	0.4	0.5	0.5	0.5	0.6	0.6	0.7	0.7	0.7	0.8	0.8
Child 002	0	0.0	0.1	0.1	0.1	0.2	0.2	0.2	0.3	0.3	0.3	0.4	0.4	0.4	0.5	0.5	0.5	0.6	0.6	0.6	0.7
Child 005	0	0.0	0.1	0.1	0.1	0.2	0.2	0.2	0.3	0.3	0.3	0.4	0.4	0.4	0.5	0.5	0.5	0.6	0.6	0.6	0.7
Child 006	0	0.0	0.1	0.1	0.2	0.2	0.2	0.3	0.3	0.4	0.4	0.4	0.5	0.5	0.6	0.6	0.6	0.7	0.7	0.8	0.8
Child 004	0	0.0	0.1	0.1	0.2	0.2	0.3	0.3	0.3	0.4	0.4	0.5	0.5	0.5	0.6	0.6	0.7	0.7	0.8	0.8	0.8
543	0	0.0	0.1	0.1	0.2	0.2	0.2	0.3	0.3	0.4	0.4	0.5	0.5	0.5	0.6	0.6	0.7	0.7	0.7	0.8	0.8
400	0	0.0	0.1	0.1	0.1	0.2	0.2	0.3	0.3	0.3	0.4	0.4	0.4	0.5	0.5	0.5	0.6	0.6	0.6	0.7	0.7
449	0	0.0	0.1	0.1	0.2	0.2	0.3	0.3	0.4	0.4	0.5	0.5	0.6	0.6	0.6	0.7	0.7	0.8	0.8	0.9	0.9
448	0	0.0	0.1	0.1	0.2	0.2	0.3	0.3	0.4	0.4	0.5	0.5	0.6	0.6	0.7	0.7	0.8	0.8	0.9	0.9	1.0
356	0	0.0	0.1	0.1	0.2	0.2	0.3	0.3	0.4	0.4	0.5	0.5	0.6	0.6	0.7	0.7	0.8	0.8	0.8	0.9	0.9
324	0	0.0	0.1	0.1	0.2	0.2	0.2	0.3	0.3	0.3	0.4	0.4	0.5	0.5	0.5	0.6	0.6	0.6	0.7	0.7	0.7

APPENDIX F – CLOSURE FORCE ANGLES AT VARYING ACTIVATION LEVELS

The closure force angles are given in degrees and muscle activation levels are in %.

Subject	0	5	10	15	20	25	30	35	40	45	50	55	60	65	70	75	80	85	90	95	100
2	0	0.3	0.5	0.8	1.0	1.3	1.5	1.8	2.0	2.3	2.6	2.8	3.1	3.3	3.6	3.9	4.1	4.4	4.6	4.9	5.2
10	0	0.0	0.1	0.1	0.2	0.2	0.3	0.3	0.4	0.4	0.5	0.5	0.6	0.6	0.7	0.7	0.7	0.8	0.8	0.9	0.9
20	0	0.0	0.0	0.0	0.0	0.0	0.0	0.0	0.0	0.0	0.0	0.0	0.0	0.0	0.0	0.0	0.0	0.0	0.0	0.0	0.0
22	0	0.1	0.1	0.2	0.2	0.3	0.3	0.4	0.4	0.5	0.6	0.6	0.7	0.7	0.8	0.8	0.9	1.0	1.0	1.1	1.1
31	0	0.0	0.1	0.1	0.2	0.2	0.3	0.3	0.3	0.4	0.4	0.5	0.5	0.6	0.6	0.7	0.7	0.7	0.8	0.8	0.9
34	0	0.1	0.1	0.2	0.3	0.3	0.4	0.5	0.5	0.6	0.7	0.7	0.8	0.9	0.9	1.0	1.1	1.2	1.2	1.3	1.4
37	0	0.1	0.3	0.4	0.5	0.6	0.8	0.9	1.0	1.1	1.3	1.4	1.5	1.7	1.8	1.9	2.0	2.2	2.3	2.4	2.6
38	0	0.2	0.3	0.5	0.6	0.8	0.9	1.1	1.3	1.4	1.6	1.7	1.9	2.0	2.2	2.4	2.5	2.7	2.8	3.0	3.1
41	0	0.2	0.3	0.5	0.7	0.8	1.0	1.2	1.3	1.5	1.6	1.8	2.0	2.1	2.3	2.5	2.6	2.8	3.0	3.1	3.3
42	0	0.1	0.2	0.3	0.5	0.6	0.7	0.8	0.9	1.0	1.1	1.3	1.4	1.5	1.6	1.7	1.8	1.9	2.1	2.2	2.3
Child 002	0	0.0	0.0	0.1	0.1	0.1	0.1	0.1	0.2	0.2	0.2	0.2	0.3	0.3	0.3	0.3	0.3	0.4	0.4	0.4	0.4
Child 005	0	0.4	0.8	1.2	1.6	2.0	2.4	2.8	3.2	3.6	4.0	4.4	4.8	5.2	5.6	5.9	6.3	6.7	7.1	7.5	7.9
Child 006	0	0.7	1.4	2.1	2.8	3.5	4.2	5.0	5.7	6.5	7.2	8.0	8.7	9.5	10.3	11.1	11.9	12.6	13.4	14.2	15.0
Child 004	0	0.0	0.1	0.1	0.2	0.2	0.3	0.3	0.4	0.4	0.5	0.5	0.6	0.6	0.7	0.7	0.7	0.8	0.8	0.9	0.9
543	0	0.0	0.0	0.1	0.1	0.1	0.1	0.1	0.2	0.2	0.2	0.2	0.3	0.3	0.3	0.3	0.3	0.4	0.4	0.4	0.4
400	0	0.1	0.2	0.3	0.4	0.5	0.6	0.7	0.8	0.9	1.0	1.1	1.2	1.3	1.4	1.5	1.7	1.8	1.9	2.0	2.1
449	0	0.1	0.2	0.3	0.5	0.6	0.7	0.8	0.9	1.0	1.1	1.3	1.4	1.5	1.6	1.7	1.8	2.0	2.1	2.2	2.3
448	0	0.0	0.0	0.0	0.0	0.0	0.0	0.0	0.0	0.0	0.0	0.0	0.0	0.0	0.0	0.0	0.0	0.0	0.0	0.0	0.0
356	0	0.1	0.1	0.2	0.3	0.4	0.4	0.5	0.6	0.7	0.7	0.8	0.9	1.0	1.0	1.1	1.2	1.3	1.4	1.4	1.5
324	0	0.0	0.0	0.0	0.0	0.0	0.0	0.0	0.0	0.0	0.0	0.0	0.0	0.0	0.0	0.0	0.0	0.0	0.0	0.0	0.0

APPENDIX G – IRB INFORMATION

No IRB was needed because data was collected for another project under an IRB #11-001103 & IRB #11099, and the data that was collected was for different purposes than that of the present study. Additionally, the data was de-identified and the investigator (Anish Sana) was not involved in subject recruitment or enrollment.